

Original Article

Cite this article: Liu J, Zhang J, Yin C-Q, Cheng C-Q, Qian J-H, Zhao C, Chen Y, Wang X, and Hsia J-Y (2021) Newly identified Jurassic–Cretaceous migmatites in the Liaodong Peninsula: unravelling a Mesozoic anatectic event related to the lithospheric thinning of the North China Craton. *Geological Magazine* **158**: 425–441. <https://doi.org/10.1017/S0016756820000552>


Received: 27 November 2019
Revised: 4 May 2020
Accepted: 7 May 2020
First published online: 30 July 2020

Keywords:

North China Craton; Liaodong Peninsula; anatexis; migmatite; lithospheric thinning

Author for correspondence: Jian Zhang,
Email: zhangjian@mail.sysu.edu.cn

Newly identified Jurassic–Cretaceous migmatites in the Liaodong Peninsula: unravelling a Mesozoic anatectic event related to the lithospheric thinning of the North China Craton

Jin Liu^{1,2} , Jian Zhang^{1,2}, Chang-Qing Yin^{1,2}, Chang-Quan Cheng^{1,2}, Jia-Hui Qian^{1,2}, Chen Zhao^{1,2}, Ying Chen^{1,2}, Xiao Wang^{1,2} and Jui-Yen Hsia^{1,2}

¹Guangdong Provincial Key Lab of Geodynamics and Geohazards, School of Earth Sciences and Engineering, Sun Yat-sen University, Guangzhou 510275, China and ²Southern Marine Science and Engineering Guangdong Laboratory (Zhuhai), Zhuhai 519000, China

Abstract

A suite of Jurassic–Cretaceous migmatites was newly identified in the Liaodong Peninsula of the eastern North China Craton (NCC). Anatexis is commonly associated with crustal thickening. However, the newly identified migmatites were formed during strong lithospheric thinning accompanied by voluminous magmatism and intense deformation. Field investigations show that the migmatites are spatially associated with low-angle detachment faults. Numerous leucosomes occur either as isolated lenses or thin layers (dykes), parallel to or cross-cutting the foliation. Peritectic minerals such as titanite and sillimanite are distributed mainly along the boundaries of reactant minerals or are accumulated along the foliation. Most zircons show distinct core–rim structures, and the rims have low Th/U ratios (0.01–0.24). Zircon U–Pb dating results indicate that the protoliths of the migmatites were either the Late Triassic (224–221 Ma) diorites or metasedimentary rocks deposited sometime after *c.* 1857 Ma. The zircon overgrowth rims record crystallization ages of 173–161 Ma and 125 Ma, which represent the formation time of leucosomes. These ages are consistent with those reported magmatic events in the Liaodong Peninsula and surrounding areas. The leucosomes indicate a strong anatectic event during the Jurassic–Cretaceous period. Partial melting occurred through the breakdown of muscovite and biotite with the presence of water-rich fluid under a thermal anomaly regime. The possible mechanism that caused the 173–161 Ma and 125 Ma anatectic events was intimately related to the regional crustal extension during the lithospheric thinning of the NCC. Meanwhile, the newly generated melts further weakened the rigidity of the crust and enhanced the extension.

1. Introduction

The North China Craton (NCC) is one of the oldest cratons (Liu *et al.* 1992; Wan *et al.* 2012) and can be divided into the Western and Eastern blocks, which collided to form the Trans-North China Orogen at *c.* 1.85 Ga (Fig. 1a; Zhao *et al.* 2005, 2012). The Eastern Block can be further divided into the Longgang Block (LGB) and Nangrim Block (NRB), separated by the Jiao–Liao–Ji Belt (JLJB) formed at *c.* 1.9 Ga (Fig. 1a; Zhao *et al.* 2005, 2012; Zhang *et al.* 2007, 2009, 2012). The Eastern NCC underwent intense lithospheric thinning and cratonic destruction during the Mesozoic Era (Zhang *et al.* 2002; Gao *et al.* 2004, 2008, 2009; Zhang, 2009; Zheng & Wu, 2009; Zhu & Zheng, 2009; Zhu *et al.* 2011, 2012a, b; Zheng *et al.* 2018), accompanied by crust-scale geological activity including magmatism (Wu *et al.* 2005), exhumation of metamorphic core complexes (MCC) and the formation of fault-bounded extensional basins (Liu *et al.* 2011, 2013). The Liaodong Peninsula is a major component of the Eastern NCC (Fig. 1a; Li *et al.* 2005, 2012), and was selected for this study because it preserves the best records of Mesozoic lithospheric thinning within the Eastern NCC (Wu *et al.* 2005; Liu *et al.* 2011, 2013).

Three major magmatic events are recognized to have occurred in the Liaodong Peninsula, during Late Triassic, Middle–Late Jurassic and Early Cretaceous time (Fig. 1b; Wu *et al.* 2005; Yang *et al.* 2007a, b; Yang & Wu, 2009; Zhang *et al.* 2014). Previous studies interpreted that the latter two events were caused by lithospheric thinning (Gao *et al.* 2008, 2009; Liu *et al.* 2008, 2011, 2013; Zhu *et al.* 2011, 2012b; Zheng *et al.* 2018). Similar magmatic activity has been reported from the Jiaodong Peninsula (Zhao *et al.* 2018). Contemporaneous structures (e.g. volcano-sedimentary basins, low-angle detachment faults and shear zones) also manifested the lithospheric thinning of the NCC (Liu *et al.* 2008, 2011, 2013). Studies of two typical

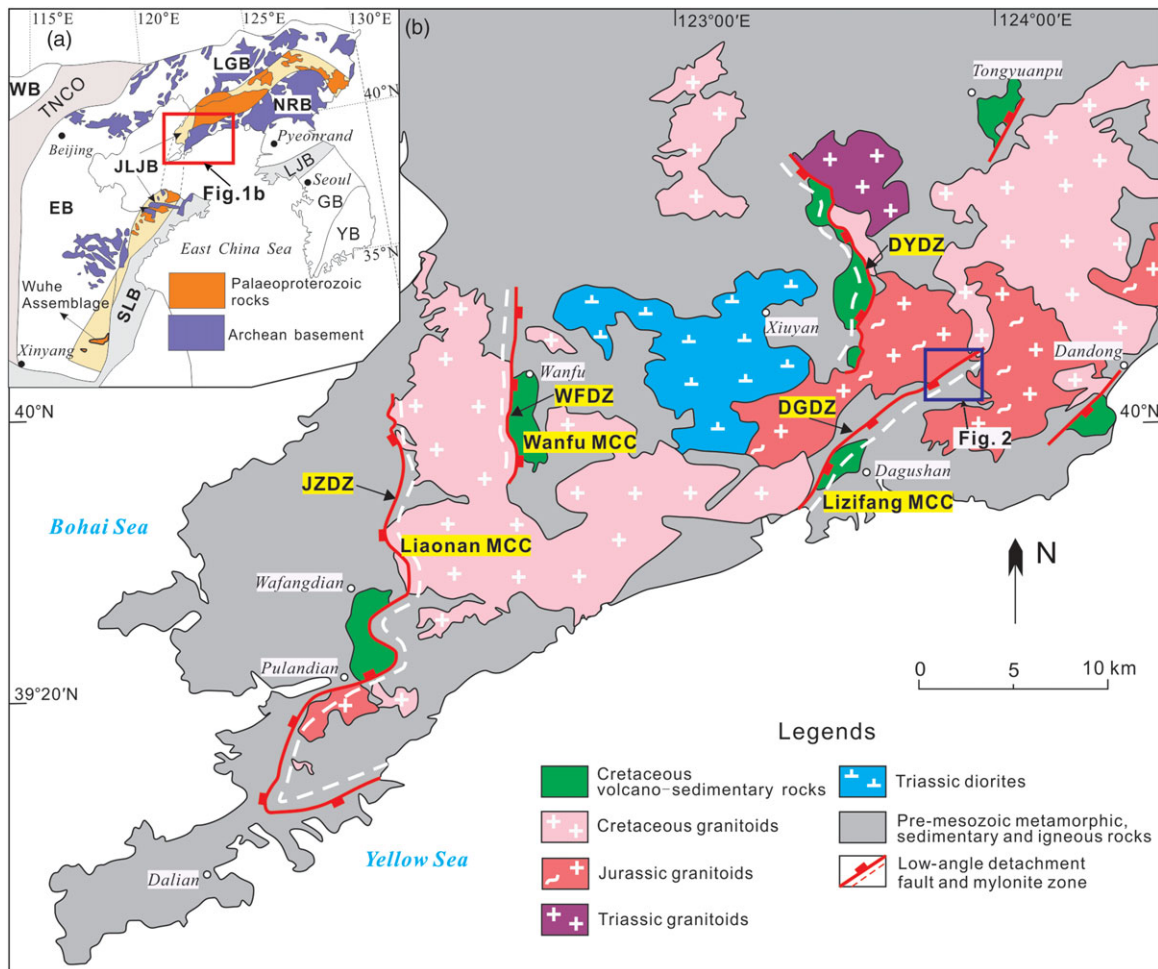


Fig. 1. (Colour online) (a) Tectonic division of the Eastern Block (after Zhao *et al.* 2005). (b) Geological sketch map of the Liaodong Peninsula (modified after Liu *et al.* 2013). WB – Western Block; EB – Eastern Block; TNCO – Trans-North China Orogen; JLJB – Jiao-Liao-Ji Belt; LGB – Longgang Block; NRB – Nangrim Block; LJB – Lmjingang Belt; GB – Gyeonggi Belt; YB – Yeongnam Block; SLB – Su-Lu Belt; JZDZ – Jinzhou detachment fault zone; WFDZ – Wanfu detachment fault zone; DYDZ – Dayingzi detachment fault zone; DGDZ – Dagushan detachment fault zone.

MCCs (Liaonan and Wanfu) indicated that the detachment of the upper-middle crust was a major driver of lithospheric thinning (Liu *et al.* 2013). Most previous studies of lithospheric thinning within the NCC mainly focused on the Mesozoic magmatism and deformation; however, very few studies have been conducted on crustal anatexis (Zhao *et al.* 2018).

Outcrops of Middle Jurassic – Lower Cretaceous migmatites have been mapped out in the Dagushan low-angle detachment fault and shear zone (DGDZ) (Fig. 2). Anatexis is generally associated with crustal thickening (Brown, 1994; Sawyer, 2001). As a partial melting product between metamorphic and igneous processes, it is an important component of crustal recycling (Brown, 2001, 2013; Sawyer, 2001, 2008; Kelsey *et al.* 2008). In the Liaodong Peninsula, the temporal and spatial distribution of the migmatites is similar to that of the DGDZ, showing an intimate link between the DGDZ and anatexis. In addition, the melts generated by anatexis can change the rheology of the continental crust (Cavalcante *et al.* 2016) and enhance the deformation. Anatexis within the DGDZ may therefore have affected rheological properties and element transport during extensional deformation and magmatism. Characterization of anatexis in the Liaodong Peninsula can provide new insights into lithospheric thinning within the NCC.

In this study, we carried out detailed field investigations, systematic petrology and geochemistry, zircon U–Pb age and Lu–Hf isotopic analysis on the newly discovered migmatites to constrain their protoliths, timing of anatexis and melting reactions. The results are combined with previous studies to elucidate the role of anatexis in the extensional deformation and crustal recycling in the Liaodong Peninsula.

2. Geological background

The Liaodong Peninsula consists of three major tectonic units: the LGB, JLJB and NRB (Fig. 1a). The oldest rocks within the NCC are 3.8–3.0 Ga tonalite–trondhjemite–granodiorite (TTG) gneisses in the Anshan area of the LGB, which were intruded by voluminous granitoids at *c.* 2.5 Ga (Liu *et al.* 1992, 2017b; Wan *et al.* 2007, 2012, 2015). In contrast, the basement of the NRB comprises mainly *c.* 2.5 Ga TTGs and Palaeoproterozoic igneous rocks (Zhai, 2016; Zhai *et al.* 2019). The basement of the JLJB mainly comprises rocks of the Palaeoproterozoic Liaohe Group and Liaoji granitoids. The Liaohe Group was deposited at 2.1–1.9 Ga, and comprises volcano-sedimentary rock units. Its lower, middle and upper parts are dominated by volcanic-, carbonate- and argillaceous-rich materials, respectively (Zhang & Yang, 1988; Luo *et al.* 2004, 2008;

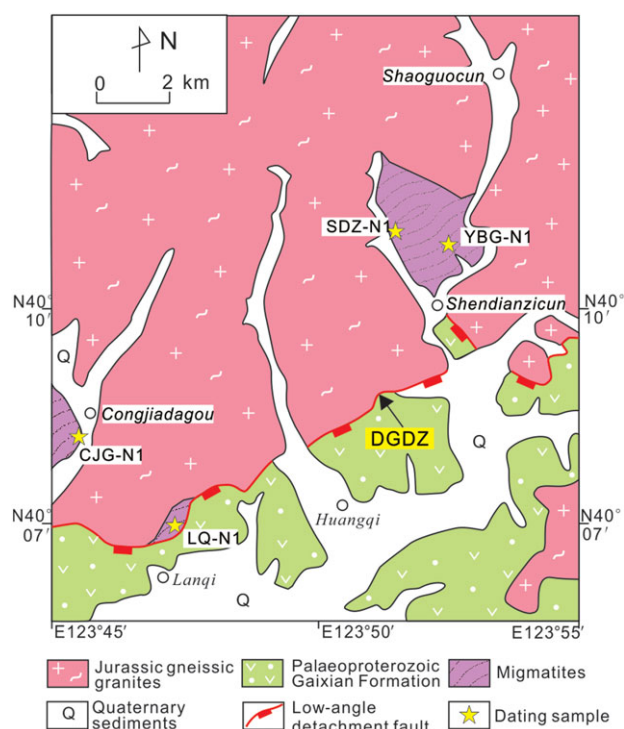


Fig. 2. (Colour online) Geological sketch map of the Shendianzi–Congjiagou area in the southeastern Liaodong Peninsula.

Liu *et al.* 2015). The Liaoji granitoids are typical A-type granites and most were emplaced at 2.2–2.1 Ga (Liu *et al.* 2018; Xu & Liu, 2019). The Liaohu Group and Liaoji granites underwent greenschist- to amphibolite-facies (locally up to granulite-facies) metamorphism at 1.90–1.85 Ga (Yin & Nie, 1996; Liu *et al.* 2015). In addition, weakly deformed or undeformed syn- and post-collision monzogranites and alkaline syenites intruded at 1900–1840 Ma, and are widespread within the southern JLJB (Lu *et al.* 2004, 2006; Liu *et al.* 2017a; Xu & Liu, 2019). Thick Neoproterozoic–Palaeozoic sedimentary sequences overlie the Liaodong Peninsula basement.

The Late Triassic (233–210 Ma) magmatism in the Liaodong Peninsula formed a large amount of granite, syenite, diorite, dolerite and lamprophyre intrusions (Fig. 1b; Wu *et al.* 2005; Yang *et al.* 2007a, b; Duan *et al.* 2014). Coeval volcanic rocks have not been reported in this area. From the Middle Jurassic to Early Cretaceous time, the eastern NCC, including the Liaodong Peninsula, underwent extensive lithospheric thinning and craton destruction, which caused voluminous magmatism and intense extensional deformation mainly at c. 125 Ma (Fig. 1b; Gao *et al.* 2008, 2009; Liu *et al.* 2008, 2011, 2013; Zhu *et al.* 2011, 2012b; Zheng *et al.* 2018). A series of low-angle detachment faults developed in the Liaodong Peninsula, including the Jinzhou, Wanfu, Dayingzi and Dagushan faults (Fig. 1b). Shearing on these detachment faults caused ductile and brittle deformation. Liu *et al.* (2013) inferred that Mesozoic extension in the Liaodong Peninsula initiated shearing along the Jinzhou detachment fault and exhumation of the Liaonan MCC before c. 134 Ma. The Lizifang MCC comprises a detachment fault (i.e. the DGDZ), a footwall of metamorphic rocks and Mesozoic granites, and a hanging wall of lower Palaeoproterozoic meta-sedimentary rocks (i.e. Gaixian Formation) and Cretaceous basins (Fig. 2; Zhong *et al.* 2019). The DGDZ is a NE-striking detachment fault that dips to the

SE at 15–30°. Abundant mylonitic and gneissic rocks are distributed within the DGDZ; among these, the Gaixian Formation consists of mica-bearing schist, fine-grained biotite-bearing gneiss and metamorphosed feldspar–quartz sandstone. The metasedimentary rocks experienced ductile deformation, characterized by sheared feldspar porphyroclasts, asymmetric folds and elongated quartz grains.

3. Field relationships and petrography

Four outcrops of migmatite (Yabagou (YBG), Shendianzi (SDZ), Lanqi (LQ) and Congjiagou (CJG)) were recently mapped out close to the NE–SW-trending DGDZ on the eastern margin of the Liaodong Peninsula (Fig. 2). Generally, the host rocks of these migmatites contain a well-developed foliation parallel to the DGDZ. These migmatites consist of leucosomes and melanosomes. The leucosomes form thin layers, veins and lenses that are parallel to, or cross-cut, the foliation (Figs 3–6). The host rocks are mainly biotite-bearing gneiss, sillimanite-bearing two-mica gneiss, orthopyroxene-bearing biotite gneiss and titanite-bearing biotite gneiss (Figs 3–6).

Outcrop YBG, close to the Yabagou Village, west of Dandong City, is dominated by sillimanite-bearing two-mica gneiss that contains plagioclase, quartz, biotite, muscovite and sillimanite with accessory zircon and opaque minerals. Geological mapping indicates that the YBG migmatite occurs as xenoliths in the wall-rock Jurassic gneissic granite. The sillimanite-bearing two-mica gneiss has a crystalloblastic texture (Fig. 3a). The host rocks of the YBG migmatite show mylonitic features in thin-section, including well-developed mylonitic foliation defined by oriented biotites, porphyroclasts of feldspar in a matrix of quartz–feldspar–mica, recrystallized feldspar and quartz ribbons (Fig. 3b–d). Some leucosome-free samples show preferred alignment, of which the clastic texture and rounded quartz and plagioclase grains indicate a sedimentary origin. On the outcrops, the YBG migmatite contains 5–10 vol% of thin leucocratic layers (most < 5 mm wide) and isolated leucosome lenses (Fig. 3a). The leucosomes occur commonly within the foliation (Fig. 3a). Biotite and muscovite are typically embayed, rounded or corroded, reflecting that they were broken down during partial melting (Fig. 3e, f). Embayed and corroded reactant minerals (e.g. biotite, muscovite, plagioclase and quartz) surround cusped patches of crystallized melt, comprising quartz, plagioclase and peritectic sillimanite (Fig. 3b–f). The crystallized melts heterogeneously distribute and occur mainly along grain boundaries. Patches of crystallized melts on the margins of adjacent reactant biotite and muscovite grains are interconnected (Fig. 3b–f). In contrast, crystallized melt trapped in the matrix of residual grains (e.g. plagioclase, quartz, biotite, muscovite) forms isolated leucocratic patches (Fig. 3a).

Migmatite outcrop LQ is located at the Lanqi Village, Dandong City. It is dominated by orthopyroxene-bearing biotite gneiss and leucocratic veins (Fig. 4a, b). Intrusive contacts between Jurassic gneissic granites and migmatites, and intrusion of gneissic granite veins into the LQ migmatite (Fig. 4a), indicate that the migmatite is a xenolith within the granite. The relict phanocrystalline texture and discontinuous foliation within the host rock might reflect an igneous origin for the protolith of the LQ migmatite. The gneissic granite and LQ migmatite display a NE-trending foliation that is parallel to the DGDZ. The leucosomes present as thin veins (0.5–2 cm wide) oriented parallel or sub-parallel to the foliation (Fig. 4b). Locally, thin leucocratic layers show a high angle to the layering (Fig. 4b), reflecting the melt coalescence and

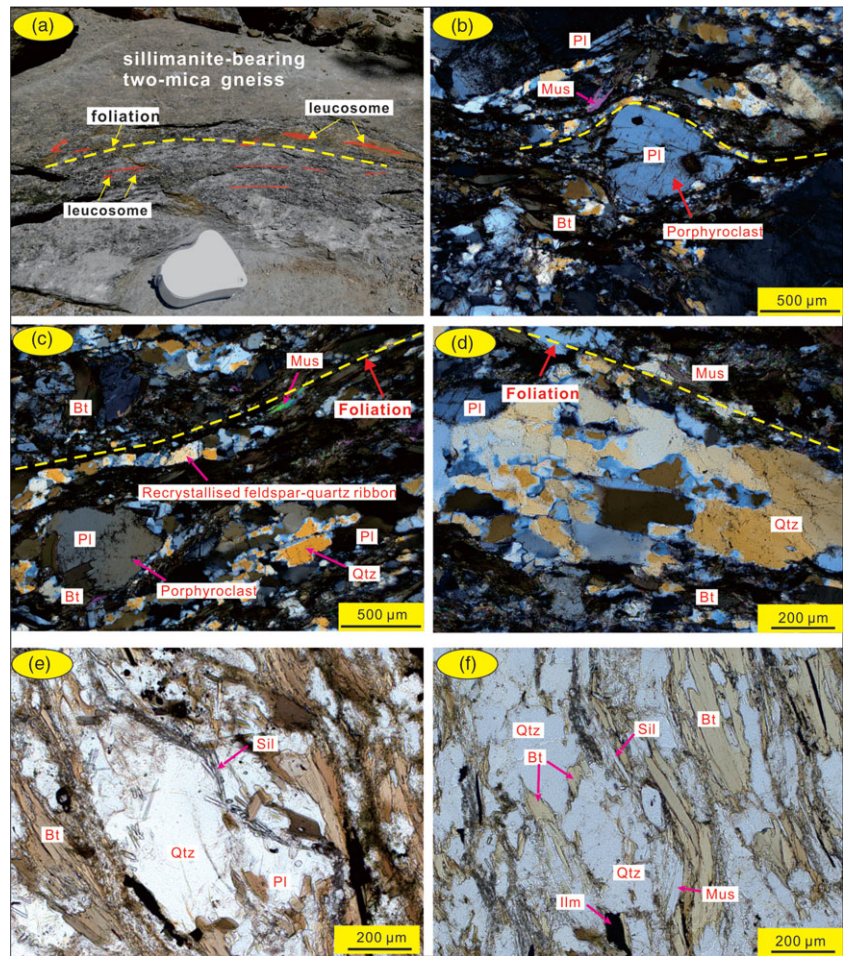


Fig. 3. (Colour online) Field photographs and microphotographs of the YBG migmatite. (a) The outcrop of YBG migmatite contains c. 5–10 vol% of thin leucocratic layer and isolated lenses, approximately distributed along the foliations. (b–d) Mylonitic features include well-developed foliation defined by orientated biotites, porphyroclasts of feldspar in a matrix of quartz-feldspar-mica, and recrystallized feldspar and quartz ribbons. (e, f) Embayed and corroded biotite and muscovite reflect breakdown during fluid-absent melting; reaction products (i.e. sillimanite, ilmenite and melt) are distributed along the boundaries of reactant minerals. Bt – biotite; Kfs – K-feldspar; Ilm – ilmenite; Pl – plagioclase; Mus – muscovite; Qtz – quartz; Sil – sillimanite.

migration. The orthopyroxene-bearing biotite gneiss comprises reactants plagioclase (50 vol%), biotite (15 vol%) and quartz (5 vol%); and reaction products orthopyroxene (5 vol%), melt (mainly quartz and plagioclase, 15 vol%), minor K-feldspar (5 vol%) and accessory minerals (total of 5 vol%; e.g. zircon and monazite) (Fig. 4c–f). The host rocks display a crystalloblastic texture and aligned biotites define a gneissic fabric (Fig. 4a, b). Partial melting is recorded by embayed and corroded biotite and plagioclase (Fig. 4c–f).

Migmatite outcrop SDZ is well-exposed in the Shendianzi Village, Dandong City. The migmatite is intruded by Jurassic gneissic granite and pegmatite (Fig. 5a, b), and comprises mainly leucosomes and biotite-bearing gneisses (Fig. 5c, d). Based on their mineralogy and features (e.g. remnant bedding and clastic textures) that reflect a sedimentary origin (Fig. 5e), the host rocks are inferred to be metagreywackes. The gradational change of the contact from the SDZ migmatite to the Gaixian Formation indicates that the migmatite used to be part of the Gaixian Formation. The leucosomes occur as two main types: (1) thin veins or layers distributed parallel to the foliation (Fig. 5c, d); and (2) broader leucocratic dykes at a high angle to the foliation (Fig. 5c, d). The two types form arrays that link the foliation planes and compositional layering. The host rocks are dominated by grey biotite-bearing gneiss with a crystalloblastic texture and a gneissic fabric defined by aligned biotite (Fig. 5f). Their mineral assemblage includes quartz (50 vol%), plagioclase (30 vol%), biotite (10 vol%) and minor epidote and titanite (5 vol%) (Fig. 5f). Epidote and titanite co-exist with the leucosomes and corroded biotites on

foliation planes (Fig. 5f), indicating that a pre-existing fabric might affect the distribution of leucosome during anatexis.

Migmatite outcrop CJG is located at the Congjiagou area of Dandong City, and is dominated by titanite-bearing biotite gneisses and leucosomes (Fig. 6a–c). Compared with the YBG and SDZ migmatites, the host rocks of the CJG migmatite show relatively discontinuous schistosity. They show a phanocrystalline texture and massive structure in some leucosome-free domains (Fig. 6d). These features indicate that the protolith of the CJG migmatite was most likely of igneous origin. The leucosomes (c. 30 vol%) occur as widespread thin veins and layers, irregular lenses and dykes (Fig. 6a–c). Three main types of leucosome occur in the CJG migmatite: (1) thin layers parallel to the foliation, inferred to have crystallized from *in situ* anatectic melts (Fig. 6b, c); (2) isolated leucocratic lenses, possibly representing *in situ* leucosomes, characterized by diffuse margins with melanosomes (Fig. 6b, c); and (3) leucocratic dykes at a high angle to the layering, propagating upwards and linking layer-parallel leucosomes (Fig. 6a–c). Sawyer (2001) suggested that high-angle discordant leucosomes like these formed last, and could represent pathways that channelled melt from melting layers. The host rocks have a crystalloblastic texture and gneissic fabric, and comprise plagioclase (45 vol%), biotite (10 vol%), quartz (15 vol%), hornblende (10 vol%), titanite (10 vol%), K-feldspar (5 vol%) and minor orthopyroxene, rutile, zircon, apatite and ilmenite (total of 5 vol%) (Fig. 6e, f). Biotite grains are embayed and corroded, consistent with biotite breakdown during anatexis. The crystallized partial melts are distributed mainly along the grain boundaries and

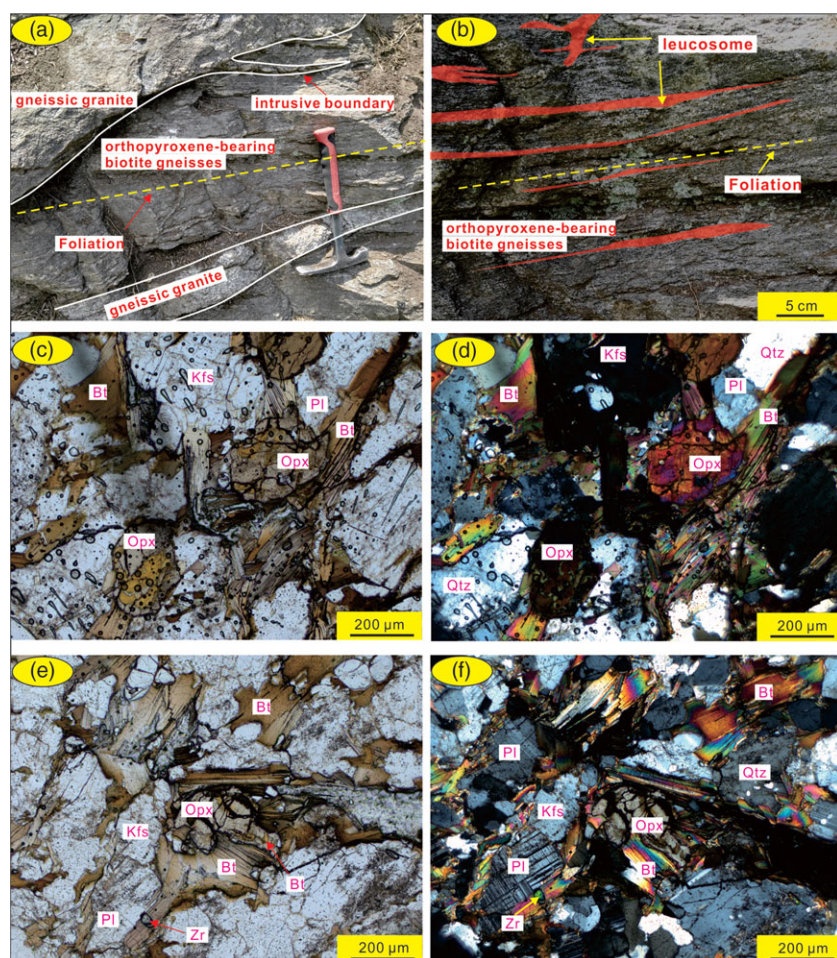


Fig. 4. (Colour online) Field photographs and microphotographs of the LQ migmatite. (a, b) The outcrop of the LQ migmatite occurs as xenolith within the Jurassic gneissic granites, and the thin leucocratic layers are distributed along the foliation. (c–f) Mineral assemblages of the LQ orthopyroxene-bearing biotite gneiss: the biotite and plagioclase are corroded by reaction products (e.g. peritectic orthopyroxene and K-feldspar and melt), mainly located at the boundaries of the reactant grains. Bt – biotite; Kfs – K-feldspar; Pl – plagioclase; Opx – orthopyroxene; Qtz – quartz; Sil – sillimanite; Zr – zircon.

are aligned parallel to the foliation (Fig. 6f). Two types of hornblende are observed in the host rocks. The first type is relatively coarse-grained and euhedral to subhedral, with inclusions of reactant minerals (e.g. biotite, quartz, plagioclase) (Fig. 6f), and is interpreted as peritectic. The other type is fine-grained with eroded margins and embayment (Fig. 6e), and is interpreted as a reactant mineral.

4. Sampling and analytical methods

Four samples (LQ-N1, SDZ-N1, YBG-N1 and CJG-N1) were selected for geochronological study from the host rocks of migmatite outcrops LQ, SDZ, YBG and CJG, respectively. Zircon grains were separated at the Langfang Regional Geological Survey, Hebei Province, China and mounted in epoxy resin. The mounts were polished to expose the grain centres, and imaged by cathodoluminescence (CL) using a CL system installed on a Quanta 200 FE-SEM at Nanjing Hongchuang GeoAnalysis, Nanjing, China. Zircon was analysed for U–Pb and Lu–Hf isotope compositions by laser ablation – inductively coupled plasma – mass spectrometry (LA-ICP-MS) at Yanduzhongshi Geological Analysis Laboratories, Beijing, China. The LA-ICP-MS operating conditions and data-reduction techniques are described by Liu *et al.* (2010). The external U–Pb standard was zircon 91500, and the Plesovice zircon was used as a secondary standard. Weighted-mean $^{206}\text{Pb}/^{238}\text{U}$ ages obtained for Plesovice zircon are consistent with the reference

value of 336.86 ± 0.76 Ma (Solari *et al.* 2010). The Lu–Hf isotopes were analysed with a Neptune-Plus multi-collector (MC-) ICP-MS instrument equipped with a NewWave UP213 laser. The laser spots for Lu–Hf analysis were 30 μm in diameter, and located as close as possible to the U–Pb analysis spots. The analytical software and correction protocols are described by Wu *et al.* (2006).

A total of 19 samples were collected from domains without leucosomes, considered to represent the mineralogical and chemical characteristics of the protoliths. Major- and trace-element analyses were undertaken at the Yanduzhongshi Geological Analysis Laboratories, Beijing, China. Fresh samples were crushed to centimetre-sized pieces, and fresh pieces selected and powdered to < 200 mesh in an agate mill. The powders were fluxed with $\text{Li}_2\text{B}_4\text{O}_7$ (1:8) at 1250°C to make homogeneous glass discs using a V8C automatic fusion machine. The glass discs were analysed for major elements by X-ray fluorescence spectrometry using an XRF-1800. The AGV-2 and GSR-1 standards were used for quality control purposes, and analytical accuracy was better than 2%. For trace-element analysis, sample powders were dissolved in distilled HF + HNO_3 in a screw-top Teflon beaker for 4 days at 100°C before analysis of the solution using an Agilent 7500 A ICP-MS instrument. The analytical precision was < 10% relative for Cr, Sc and Sr, and < 5% relative for other elements. The GSR-2 standard was used for quality control purposes and its analysis results were consistent with reference values. Further details of the analytical procedure are provided by Qi *et al.* (2000).

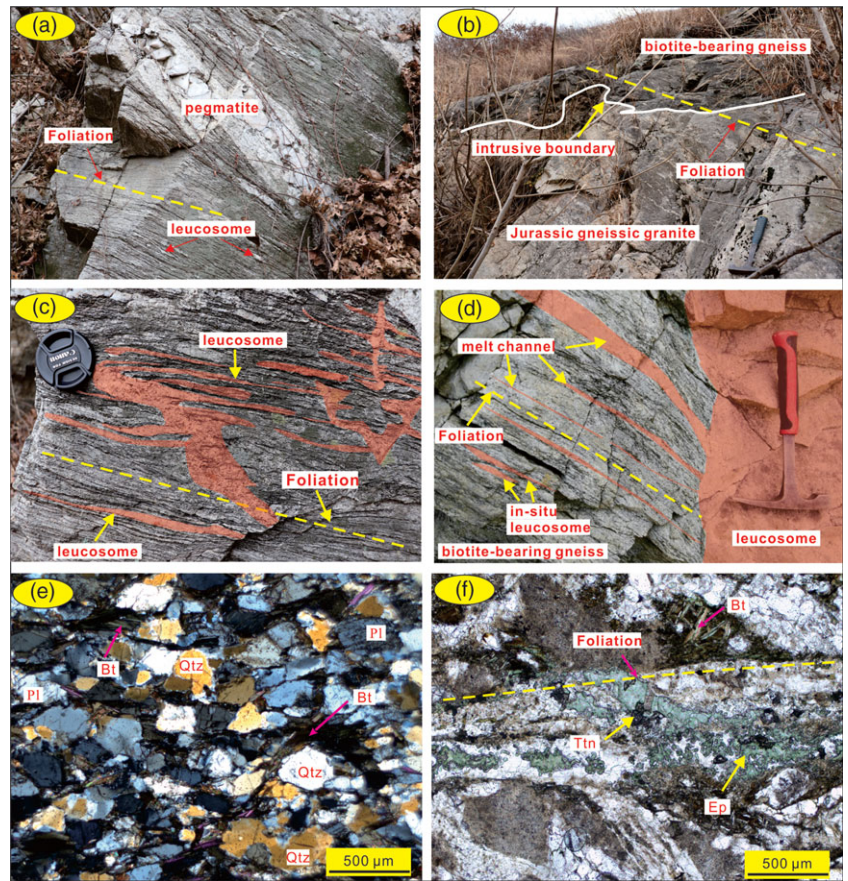


Fig. 5. (Colour online) Field photographs and microphotographs of the SDZ migmatite. (a, b) The Jurassic gneissic granite and pegmatite intruded into the SDZ migmatite. (c, d) The thin vein or layer distributed parallel to the foliation; in contrast, wider and oblique leucocratic dykes that are oriented at a high angle to the foliation reflect linked arrays along the plane of the foliation and compositional layering. (e) Mineral assemblages show remnant clastic textures in some leucosome-free domains. (f) Mineral assemblages of the SDZ biotite-bearing gneiss: the peritectic epidotes and titanites together with felsic melts are mainly located along the foliation, where biotites are apparently corroded. Bt – biotite; Ep – epidote; Pl – plagioclase; Qtz – quartz; Ttn – titanite.

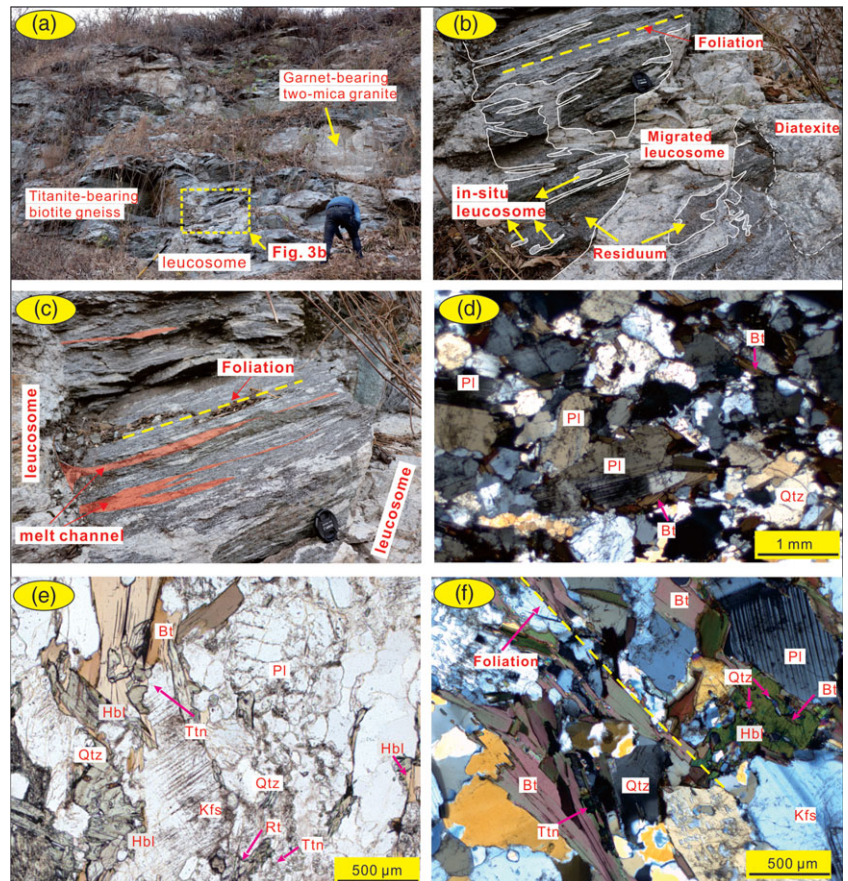


Fig. 6. (Colour online) Field photographs and microphotographs of the CJG migmatite. (a–c) The CJG migmatite contains c. 30 vol% leucosomes, which are mainly present as thin layers parallel to the foliation, isolated *in situ* leucocratic lenses and high-angle leucocratic dykes. (d) Mineral assemblages show phanocrystalline textures in some leucosome-free domains. (e, f) Mineral assemblages of the CJG titanite-bearing biotite gneiss: biotite grains are featured by embayed and corroded shapes, which reflecting biotite breakdown during anatexis. The anatectic melts and peritectic minerals (e.g. hornblende, titanite, rutile and orthopyroxene) are mainly distributed along the grain boundaries at a grain-scale and parallel to the principal fabric (i.e. foliation). Bt – biotite; Hbl – hornblende; Kfs – K-feldspar; Pl – plagioclase; Opx – orthopyroxene; Qtz – quartz; Ttn – titanite; Rt – rutile.

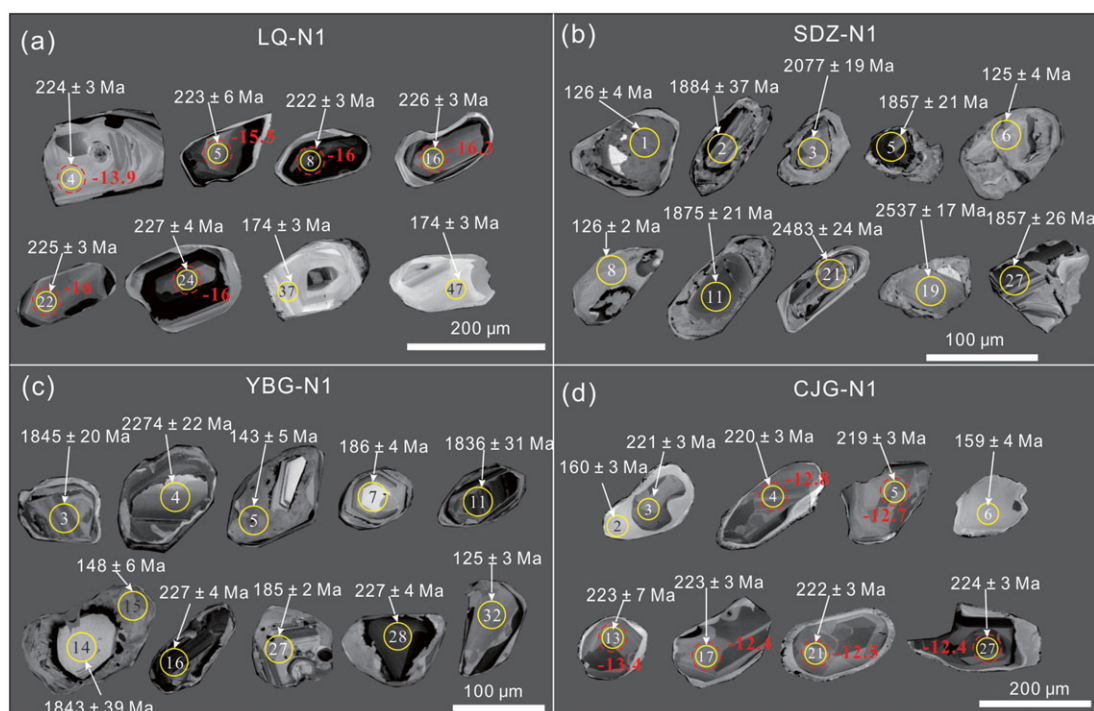


Fig. 7. (Colour online) CL images of representative zircons from the host rocks showing internal textures.

5. Results

5.a. Zircon U–Pb geochronology

5.a.1. Sample LQ-N1

Sample LQ-N1 is an orthopyroxene-bearing biotite gneiss of the LQ migmatite. Zircons from this sample are typically 100–200 μm in diameter with aspect ratios of 1–2. They are irregular or prismatic and typically exhibit distinct cores and rims in CL images (Fig. 7a). Most zircon cores display oscillatory zonation, but the rims have little internal structure and are homogeneous or display blurred oscillatory zoning (Fig. 7a). Yakymchuk & Brown (2014) proposed that some zircons are expected to survive heating to peak temperature, and new zircons grow subsequently from melt trapped along grain boundaries during cooling to the solidus. The zircon cores are therefore inferred to be sourced from the protolith and the rims to have formed during anatexis. A total of 33 analyses of the zircon cores yielded tightly clustered $^{206}\text{Pb}/^{238}\text{U}$ ages of 228–220 Ma and high Th/U ratios of 0.33–1.02 (online Supplementary Table S1, available at <http://journals.cambridge.org/geo>). Most zircon core analyses are concordant (concordance > 99%) and yield a weighted-mean $^{206}\text{Pb}/^{238}\text{U}$ age of 224 ± 2 Ma (Fig. 8a), which is interpreted as the crystallization age of the protolith. The eight rim analyses have low Th/U ratios (0.06–0.26) and tightly clustered $^{206}\text{Pb}/^{238}\text{U}$ ages of 176–171 Ma, with a weighted-mean age of 173 ± 2 Ma (Fig. 8a) that is interpreted as the age of zircon growth during anatexis.

5.a.2. Sample SDZ-N1

Sample SDZ-N1 is a biotite-bearing gneiss from the SDZ migmatite. Zircons from the sample are < 100 μm in diameter. CL images indicate distinct cores and rims (Fig. 7b). Zircon cores have complex structures, including concentric oscillatory, banded, planar and blurred zones (Fig. 7b), indicative of a detrital origin. In

contrast, the rims are relatively bright and display homogeneous zoning, indicative of an anatectic origin. The zircon rims have low Th/U ratios (0.01–0.05). Seven analyses of the zircon rims yielded $^{206}\text{Pb}/^{238}\text{U}$ ages of 126–122 Ma and a weighted-mean age of 125 ± 2 Ma (Fig. 8b), interpreted as the age of zircon growth during anatexis. The zircon cores yielded variable $^{207}\text{Pb}/^{206}\text{Pb}$ ages of 2537–1857 Ma and Th/U ratios of 0.03–1.24 (online Supplementary Table S1). The most common age recorded by the zircon cores is 1921–1857 Ma, followed by ages of 2537–2411 Ma (Fig. 8b). Five zircon cores with ages of 1.92–1.87 Ga have extremely low Th/U ratios of 0.03–0.07 (online Supplementary Table S1) and CL images with blurred or fan oscillatory zones, consistent with a metamorphic origin.

5.a.3. Sample YBG-N1

Sample YBG-N1 is a sillimanite-bearing two-mica gneiss of the YBG migmatite. Zircons from this sample are typically 80–150 μm in diameter, and most have distinct cores and rims (Fig. 7c). The zircon cores can be divided into two groups. Some show clear concentric oscillatory or banded zoning and relatively high Th/U values of 0.21–1.38 (online Supplementary Table S1), indicative of an igneous origin, whereas others show blurred oscillatory zoning and relatively low Th/U ratios of 0.04–0.17 (online Supplementary Table S1), indicative of a metamorphic origin. The zircon rims display homogeneous zoning with low Th/U ratios of 0.01–0.03 (online Supplementary Table S1), indicative of an anatectic origin. A total of 22 zircon cores yielded variable ages of 2536–1830 Ma and nine analyses yielded ages of 227–142 Ma, interpreted as mixed ages. A group of zircon cores with ages that range from 1937 to 1830 Ma yield a peak at 1855 Ma (Fig. 7c), whereas the older dates range from 2536 to 1992 Ma. Seven analyses of the zircon rims yielded $^{206}\text{Pb}/^{238}\text{U}$ ages of 127–121 Ma with a weighted-mean age of

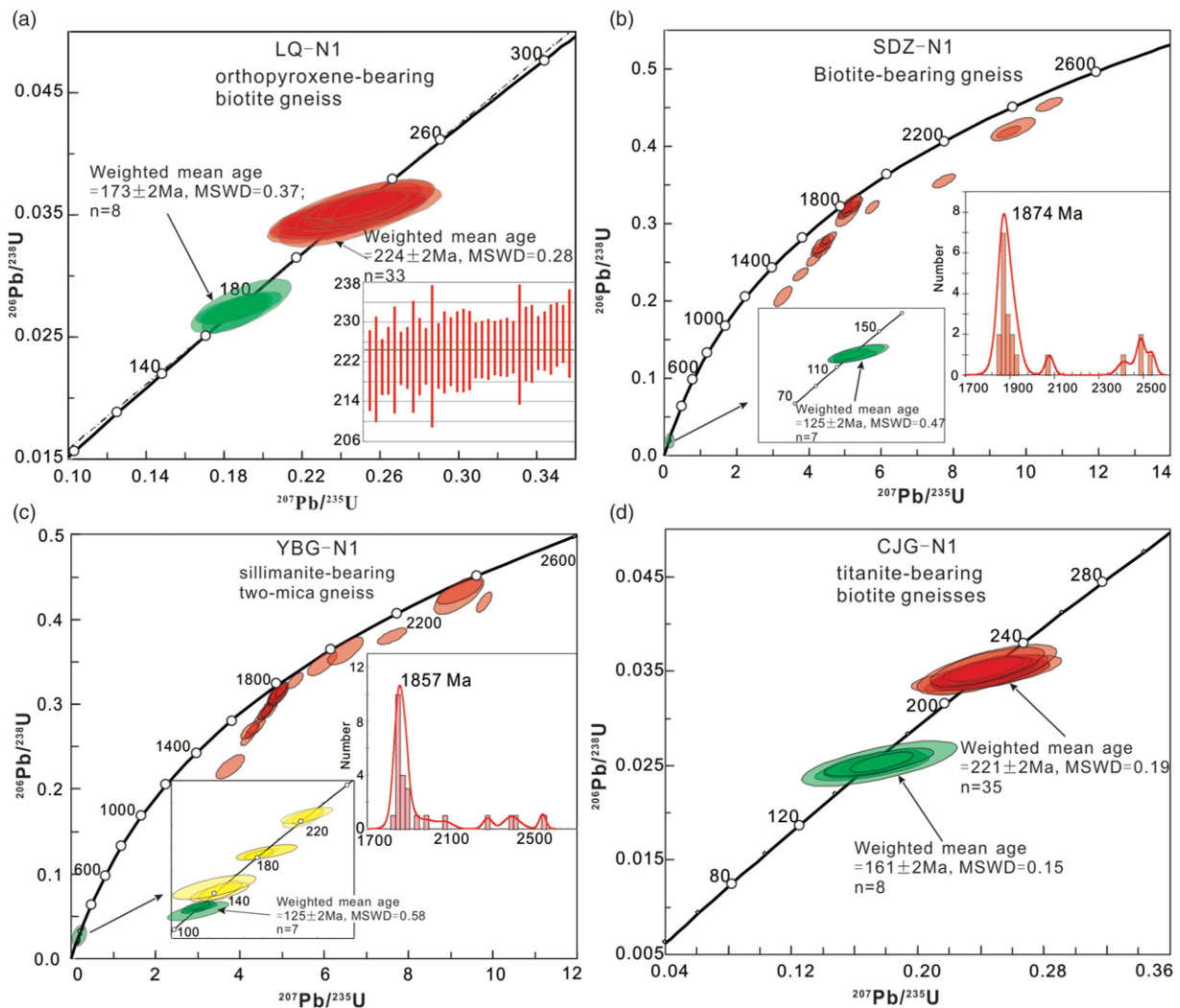


Fig. 8. (Colour online) LA-ICP-MS zircon U-Pb dating concordia diagrams for the samples of the host rocks.

125 ± 2 Ma (Fig. 8c), interpreted as the age of zircon growth during anatexis.

5.a.4. Sample CJG-N1

Sample CJG-N1 is a titanite-bearing biotite gneiss of the CJG migmatite. Most zircons from this sample display typical core-rim structures and are 100–200 μm in size (Fig. 7d). Zircon cores have clear and wide oscillatory zoning (Fig. 7d) and high Th/U ratios (0.55–1.22), whereas the rims have homogeneous or blurred oscillatory zoning and lower Th/U values of 0.11–0.77 (Fig. 7d). The zircon cores are inferred to be magmatic, but the rims have relatively higher Th/U values than the zircons that formed during anatexis (generally < 0.1). Previous studies suggested that anatectic zircons with high Th/U values could be formed by recrystallization under fluid-rich conditions (Pidgeon, 1992; Rubatto & Hermann, 2003; Dong *et al.* 2017). These zircon rims are therefore inferred to have formed during anatexis. A total of 35 analyses of the zircon cores yielded tightly clustered $^{206}\text{Pb}/^{238}\text{U}$ ages of 225–217 Ma with a weighted-mean $^{206}\text{Pb}/^{238}\text{U}$ age of 221 ± 2 Ma (Fig. 8d; online Supplementary Table S1), interpreted as the crystallization age of the protolith. Eight zircon rim analyses yielded $^{206}\text{Pb}/^{238}\text{U}$ ages of 162–159 Ma with a weighted-mean age of 161 ± 2 Ma (Fig. 8d;

online Supplementary Table S1), interpreted as the age of zircon growth during anatexis.

5.b. Whole-rock major- and trace-element data

The geochronological data record tightly clustered Triassic ages and an igneous origin for the protoliths of samples LQ-N1 and CJG-N1 (*c.* 220 Ma; Fig. 8a, d). In contrast, the age spectra of samples SDZ-N1 and YBG-N1 are characteristic of sedimentary rocks with depositional ages younger than *c.* 1857 Ma (Fig. 8b, c).

The protoliths of metamorphic rocks can also be constrained by their geochemistry (Simonen, 1953; McLennan *et al.* 1990). The protoliths of the LQ and CJG migmatites plot in the field of volcanic rocks in the ((Al + fm) - (c + alk)) - Si diagram (Fig. 9a), consistent with an igneous origin. In contrast, the protoliths of the SDZ and YBG migmatites plot nearer the field of sedimentary rocks (Fig. 9a), consistent with a sedimentary origin. Furthermore, the SDZ and YBG migmatites plot in the sandstone and greywacke fields in the (La/Yb) - (ΣREE) diagram (ΣREE is total rare-earth element content) (Fig. 9b). These findings are consistent with the protoliths inferred from the geochronological results and field observations.

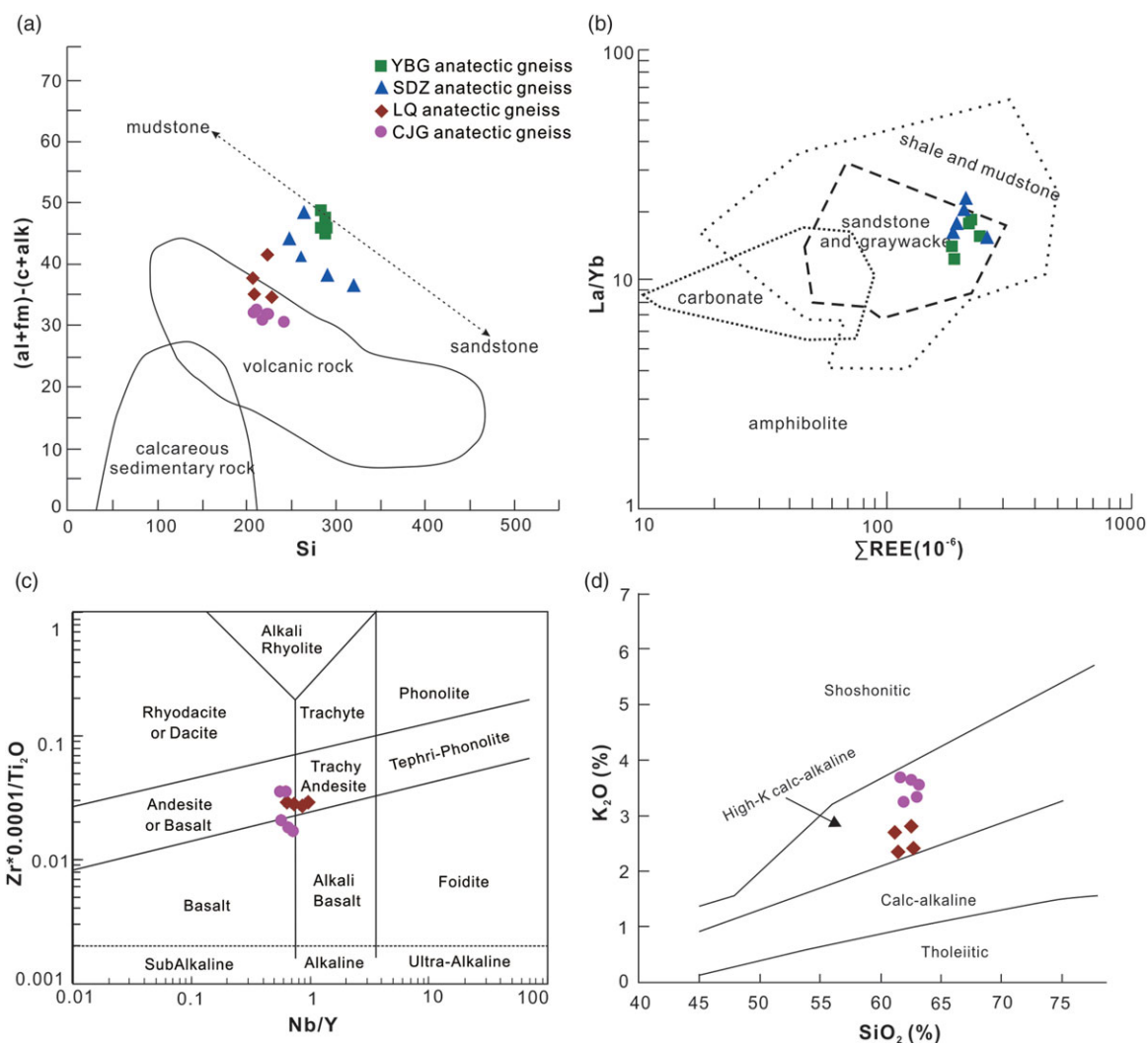


Fig. 9. (Colour online) (a) $(al + fm) - (c + alk)$ v. Si diagram (after Simonen, 1953); (b) (La/Yb) v. ΣREE diagram (after Wang *et al.* 1987); (c) Nb/Y v. Zr/TiO_2 geochemical classification diagram (Winchester & Floyd, 1977); (d) K_2O v. SiO_2 (Rickwood, 1989). $\Sigma = Al_2O_3 + 2Fe_2O_3 + FeO + MgO + MnO + CaO + Na_2O + K_2O$; $al = (Al_2O_3/\Sigma) \times 100$; $fm = (2Fe_2O_3 + FeO + MgO + MnO)/\Sigma \times 100$; $c = (CaO/\Sigma) \times 100$; $alk = (Na_2O + K_2O)/\Sigma \times 100$; $al + fm + c + alk = 100$; $Si = (SiO_2/\Sigma) \times 100$.

5.b.1. SDZ and YBG migmatites

Many geochemical features of the SDZ and YBG hosts are similar. The samples have relatively high SiO_2 (62.27–69.59 wt %) and CaO (1.38–2.08 wt %) contents, and low total Fe_2O_3 (4.73–6.47 wt %) and K_2O (2.89–3.66 wt %) contents (online Supplementary Table S2, available at <http://journals.cambridge.org/geo>). They have relatively high ΣREE contents of 182.0–252.2 ppm (online Supplementary Table S2), and are slightly enriched in light REE (LREE) ($(La/Yb)_N = 8.81$ –15.94) with strongly negative Eu anomalies ($Eu/Eu^* = 0.45$ –0.56) (Fig. 10a). Previous studies concluded that the protoliths of these migmatites are sedimentary rocks, and this interpretation is supported by a comparison of the trace-element characteristics of these samples with those of the upper continental crust (UCC) (Fig. 10b). The SDZ and YBG migmatite samples are enriched in large-ion lithophile elements (LILEs; e.g. Rb, Ba and Th), depleted in the high-field-strength elements (HFSEs; e.g. Nb, Ta, Ti and P) and plot near the UCC in the primitive-mantle-normalized multi-element diagram (Fig. 10b).

5.b.2. LQ and CJG migmatites

Samples of the LQ and CJG hosts also share similar geochemical features. They plot in the basalt–andesite field in the $(Nb/Y) - (Zr/TiO_2)$ diagram (Fig. 9c) and have moderate SiO_2 (61.19–63.14 wt %) and total Fe_2O_3 (4.42–5.74 wt %) contents and relatively high Al_2O_3 (15.16–17.05 wt %), MgO (3.36–4.55 wt %) and CaO (3.93–4.75 wt %) contents (online Supplementary Table S2). On oxide versus SiO_2 diagrams (Fig. 11), SiO_2 shows linear correlations with MgO , total Fe_2O_3 , TiO_2 and P_2O_5 . The Mg numbers are relatively high (58–65), K_2O/Na_2O ratios low (0.73–1.26) and A/CNK ratios variable (0.90–1.18) (online Supplementary Table S2). Most of the samples plot in the high-K calc-alkaline field in the $K_2O - SiO_2$ diagram (Fig. 9d). Their ΣREE contents (229.7–400.8 ppm) are high, with small negative Eu anomalies ($Eu/Eu^* = 0.65$ –0.84). They are enriched in LREE ($(La/Yb)_N = 39.26$ –81.21) and strongly depleted in HREE in the chondrite-normalized multi-element diagram (Fig. 10c; online Supplementary Table S2). The samples are also enriched in LILEs (e.g. Rb, Ba and Th) and depleted in HFSEs (e.g. Nb, Ta, Ti and P) relative to the primitive mantle (Fig. 10d).

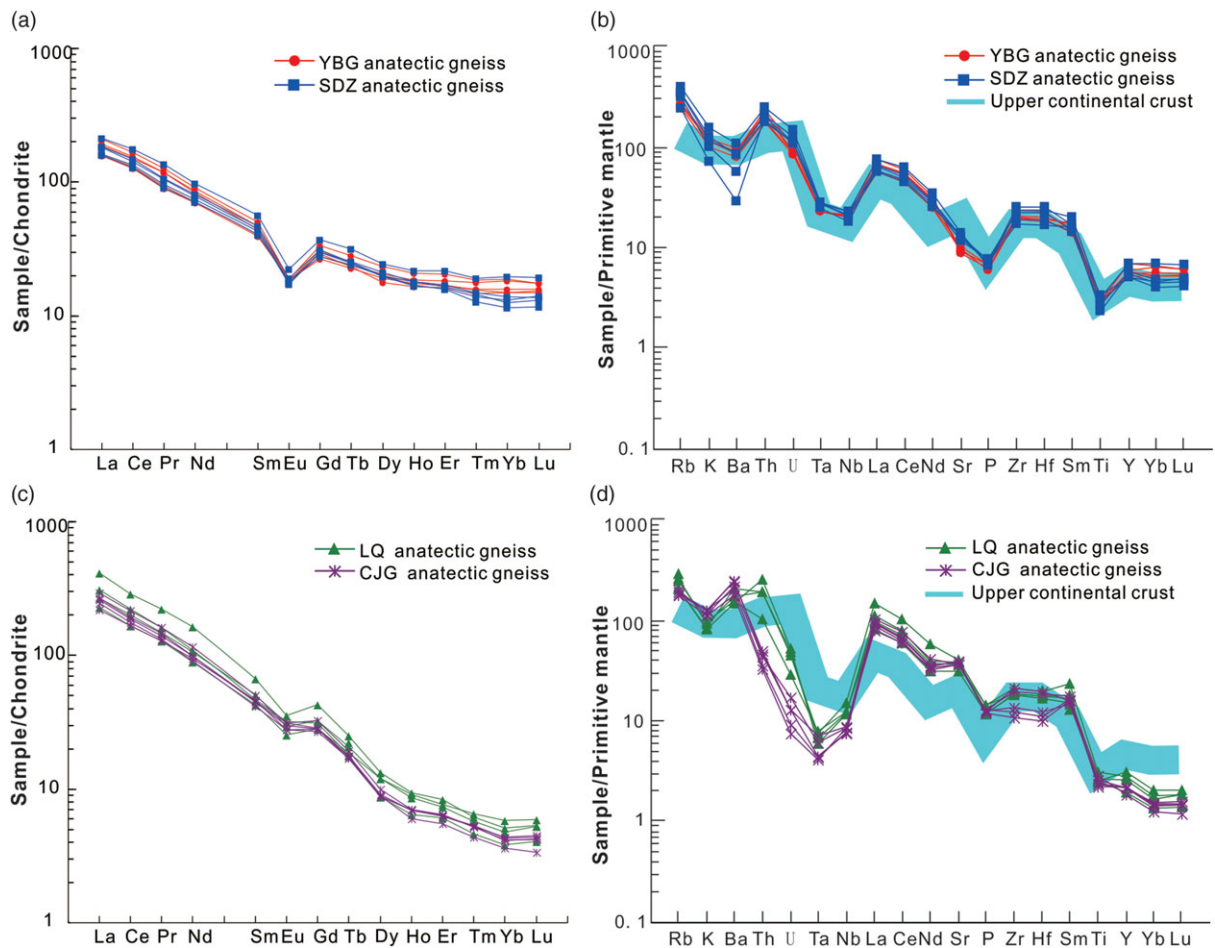


Fig. 10. (Colour online) (a, c) Chondrite-normalized REE and (b, d) primitive mantle-normalized trace-element spider diagrams for the samples. The data for chondrite and primitive mantle-normalized are from Sun & McDonough (1989), and the upper continental crust values are from Rudnick & Gao (2003).

5.c. Zircon Lu–Hf isotopic compositions

The Lu–Hf isotopic compositions of zircon cores from samples LQ-N1 and CJG-N1 were determined *in situ* (Table 1) and are similar and relatively homogeneous (excluding analysis CJG-N1-34). The initial $^{176}\text{Hf}/^{177}\text{Hf}$ and $^{176}\text{Lu}/^{177}\text{Hf}$ ratios are in the ranges 0.282174–0.282294 and 0.000157–0.000631, respectively. The $\epsilon_{\text{Hf}}(t)$ values are negative (–16.3 to –12.1) and yield two-stage Hf model ages ($T_{\text{DM}2}$) of 2282–2016 Ma (Table 1). Analysis CJG-N1-34 records a relatively low initial $^{176}\text{Hf}/^{177}\text{Hf}$ ratio (0.282033) and $\epsilon_{\text{Hf}}(t)$ value (–21.3) and a high value of $T_{\text{DM}2}$ (*c.* 2593 Ma; Table 1).

6. Discussion

6.a. Depositional age and provenance of protoliths of SDZ and YBG migmatites

The youngest group of detrital zircons from samples SDZ-N1 and YBG-N1 has age peaks at 1874 and 1857 Ma (Fig. 8b, c), respectively. The depositional age is therefore younger than *c.* 1857 Ma, but older than the age of leucosome crystallization at 125 ± 2 Ma.

Samples SDZ-N1 and YBG-N1 have distinctly different age spectra to metasedimentary rocks of the Liaohe Group (Fig. 12). For example, the largest age peaks in samples SDZ-N1 and YBG-N1 (1937–1830 Ma) are different to those of Liaohe Group samples (Fig. 12). The depositional age of the Liaohe Group

is *c.* 2.0–1.9 Ga (Li *et al.* 2015; Liu *et al.* 2018), older than the depositional age of the protolith of SDZ-N1 and YBG-N1. It has recently been suggested that metasedimentary rocks of the SE Liaodong Peninsula, which were thought to be part of the Gaixian Formation, were deposited after the Liaohe Group (Meng *et al.* 2013; Wang *et al.* 2018). The most common age of detrital grains in metasedimentary rocks from the Changhai Island is 1916–1856 Ma, with a peak at *c.* 1887 Ma (Meng *et al.* 2013). Wang *et al.* (2018) also reported an age peak at *c.* 1863 Ma for a metamorphosed feldspar–quartz sandstone from the SE Liaodong Peninsula, which was previously thought to be part of the Gaixian Formation. The detrital zircon age spectra of samples SDZ-N1 and YBG-N1 are similar to those of metasedimentary rocks from the SE Liaodong Peninsula (Fig. 12). A suite of Palaeoproterozoic metasedimentary rocks is widely exposed in the eastern part of the DGDZ (Fig. 2). They have similar lithological and deformational characteristics to the metasedimentary rocks reported by Meng *et al.* (2013) and Wang *et al.* (2018). The protolith of the SDZ and YBG migmatites may therefore be related to these metasedimentary rocks, rather than the Liaohe Group.

Strong magmatic–hydrothermal activity was widespread in the SE Liaodong Peninsula at 1.90–1.85 Ga. Late Palaeoproterozoic rocks formed there at that time have been studied in detail. These include the Kuangdonggou syenite (1.87–1.85 Ga; Cai *et al.* 2002; Yang *et al.* 2007c), Tonghua diorite–monzogranite–syenite complex (1.87–1.85 Ga; Liu *et al.* 2017a) and Qingchengzi

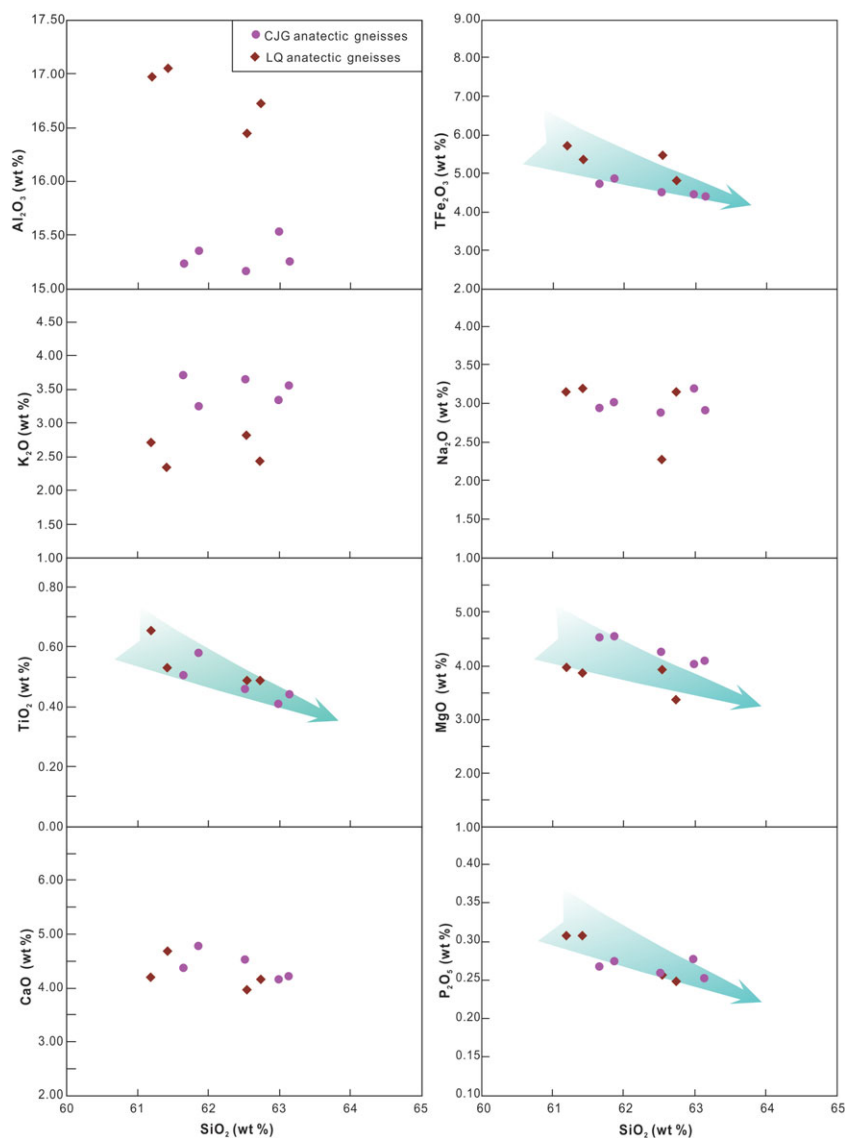


Fig. 11. (Colour online) Major oxides v. SiO_2 for the C.J.G. and L.Q. anatectic gneisses.

granite (c. 1.89 Ga; Wang *et al.* 2017). It is likely that the 1921–1857 Ma zircon grains from sample SDZ-N1 and YBG-N1 were derived from these late Palaeoproterozoic (1.90–1.85 Ga) igneous rocks. In addition, five zircon cores with metamorphic origin yield ages of c. 1.92–1.87 Ga, which are consistent with the metamorphic ages of the Liaohe Group (Fig. 12; Yin & Nie, 1996; Liu *et al.* 2015, 2018). These five zircons may therefore be sourced from the Liaohe Group. Other zircon ages of 2.5–2.1 Ga are consistent with those of NCC crystalline basement in the Liaodong Peninsula, such as the Palaeoproterozoic Liaoji granites (2.2–2.1 Ga; Liu *et al.* 2018) and Neoproterozoic TTGs (2.7–2.5 Ga) (Wan *et al.* 2015; Wang *et al.* 2016). It is therefore likely that some zircons were derived from the crystalline basement.

6.b. Petrogenesis of the protoliths of LQ and C.J.G. migmatites

Petrological, geochemical and geochronological data indicate that the protoliths of the LQ and C.J.G. migmatites were igneous rocks. However, these data do not reveal whether the igneous rocks were intrusive or extrusive. The protolith of the LQ and C.J.G. migmatites formed during Late Triassic time (c. 220 Ma). A number of Late

Triassic plutons are recognized in the Liaodong Peninsula (Fig. 1b; Table 2), including the Saima–Bolinchuan nepheline syenite (233–231 Ma; Wu *et al.* 2005), Xiuyan granite and associated mafic microgranular enclaves (213–210 Ma; Wu *et al.* 2005; Yang *et al.* 2007b), Yujiacun syenite (221 Ma; Wu *et al.* 2005), Yinjiacun and Daheshangshan dolerites (213–212 Ma; Yang *et al.* 2007a), Shuangdinggou granite (224 Ma; Duan *et al.* 2014) and Qingchengzi lamprophyre (227–210 Ma; Duan *et al.* 2014). Triassic volcanic rocks have not been reported. Based on this observation and the geochemistry, the protoliths of the LQ and C.J.G. migmatites are inferred to have been the Late Triassic intrusive rocks, which can be further classified as diorites in the Nb/Y versus Zr/TiO₂ diagram (Fig. 9c).

The LQ and C.J.G. diorites have moderate SiO_2 , $\text{K}_2\text{O} + \text{Na}_2\text{O}$, total Fe_2O_3 and Al_2O_3 contents, consistent with a crustal origin. Their MgO (3.36–4.55 wt%) and CaO (3.93–4.75 wt%) contents and Mg number values (58–65) are relatively high, possibly recording the addition of mantle materials and/or fractional crystallization. The systematic variations in SiO_2 , MgO, total Fe_2O_3 , TiO_2 and P_2O_5 contents (Fig. 11) are consistent with fractionation of amphibole, rutile and apatite. Previous studies on the coeval

Table 1. Zircon Hf isotopic data for the sample LQ-N1 and CJG-N1

Test no.	Age (Ma)	$^{176}\text{Yb}/^{177}\text{Hf}$	$^{176}\text{Lu}/^{177}\text{Hf}$	$^{176}\text{Hf}/^{177}\text{Hf}$	$\epsilon_{\text{Hf}}(t)$	2σ	T_{DM1}	T_{DM2}	$f_{\text{Lu/Hf}}$
LQ-N1									
04	224	0.012721	0.000363	0.282242	-13.9	0.57	1403	2132	-0.99
05	224	0.010472	0.000311	0.282197	-15.5	0.42	1462	2231	-0.99
08	224	0.010434	0.000326	0.282183	-16.0	0.49	1482	2262	-0.99
09	224	0.017266	0.000493	0.282218	-14.7	0.44	1440	2185	-0.99
14	224	0.009764	0.000283	0.282243	-13.8	0.43	1398	2127	-0.99
15	224	0.008787	0.000263	0.282189	-15.8	0.41	1471	2248	-0.99
16	224	0.011050	0.000334	0.282174	-16.3	0.44	1494	2282	-0.99
20	224	0.022195	0.000631	0.282201	-15.4	0.47	1469	2224	-0.98
22	224	0.018994	0.000544	0.282183	-16.0	0.40	1490	2263	-0.98
24	224	0.013577	0.000400	0.282182	-16.0	0.49	1486	2264	-0.99
26	224	0.015302	0.000441	0.282204	-15.3	0.46	1458	2217	-0.99
31	224	0.011654	0.000375	0.282227	-14.4	0.47	1424	2165	-0.99
34	224	0.005874	0.000173	0.282033	-21.3	0.80	1680	2593	-0.99
CJG-N1									
01	221	0.009392	0.000265	0.282268	-13.0	0.43	1364	2075	-0.99
04	221	0.007956	0.000228	0.282273	-12.8	0.46	1355	2062	-0.99
05	221	0.008981	0.000272	0.282276	-12.7	0.53	1352	2056	-0.99
09	221	0.005937	0.000172	0.282278	-12.6	0.42	1346	2050	-0.99
13	221	0.008713	0.000249	0.282257	-13.4	0.44	1378	2098	-0.99
14	221	0.007269	0.000213	0.282291	-12.2	0.43	1330	2022	-0.99
17	221	0.008997	0.000252	0.282286	-12.4	0.47	1338	2035	-0.99
21	221	0.007690	0.000219	0.282282	-12.5	0.48	1342	2042	-0.99
27	221	0.009219	0.000263	0.282285	-12.4	0.45	1340	2036	-0.99
31	221	0.011464	0.000309	0.282291	-12.2	0.45	1333	2023	-0.99
35	221	0.006410	0.000184	0.282252	-13.6	0.54	1383	2110	-0.99
40	221	0.005445	0.000157	0.282294	-12.1	0.51	1324	2016	-1.00
42	221	0.008097	0.000229	0.282274	-12.8	0.55	1354	2062	-0.99
46	221	0.009036	0.000247	0.282253	-13.6	0.48	1384	2108	-0.99

Xiuyan granitoids and their mafic enclaves (Yang *et al.* 2007b) and the Daheikeng diorites (Wang *et al.* 2019) in adjacent regions have revealed that mantle- and crust-derived magma mixing was a common feature of the Late Triassic magmatism in the Liaodong Peninsula. The high MgO and CaO contents and Mg number values of the LQ and CJG diorites may therefore reflect a contribution by mantle materials. Zircons from the LQ and CJG diorites have negative $\epsilon_{\text{Hf}}(t)$ values (-16.3 to -12.1; Table 1), indicating the parent magmas were partial melts of recycled ancient crust. The old T_{DM2} ages (2282–2016 Ma) are also consistent with derivation of the parent magmas from mafic Palaeoproterozoic crustal material. The *c.* 2.1 Ga mafic rocks of the JLJB have high positive $\epsilon_{\text{Hf}}(t)$ values (Meng *et al.* 2014; Fig. 13) consistent with derivation directly from depleted mantle. The Hf isotopic compositions of the proposed diorite protoliths of the LQ and CJG rocks and the *c.* 2.12 Ga mafic rocks are similar (Fig. 13), implying that the mafic rocks melted to form the parental magma of the LQ and CJG diorites. Other Upper Triassic intrusive rocks within the Liaodong Peninsula have similar Hf isotopic compositions to the LQ and CJG

samples (Yang *et al.* 2007a, b; Duan *et al.* 2014; Fig. 13), indicating that they share a common source. Furthermore, the LQ and CJG rocks have high Sr/Y ratios (46.5–90.2) and are HREE-depleted (Fig. 10), indicating that garnet was a residual phase in the magma source region. Yang *et al.* (2007a, b, 2012) inferred that delamination of thickened continental crust caused the Late Triassic magmatism in the Liaodong Peninsula. Based on the above, it is concluded that the parental magmas of the LQ and CJG protoliths were partial melts of thickened Palaeoproterozoic mafic lower crust that were mixed with mantle-derived magma and experienced fractional crystallization during ascent.

6.c. Relationship between Jurassic–Cretaceous anatexis and lithospheric thinning

There is consensus that the eastern NCC underwent lithospheric thinning and craton destruction during the Mesozoic Era (Zhang *et al.* 2002; Gao *et al.* 2004, 2008, 2009; Zhang, 2009;

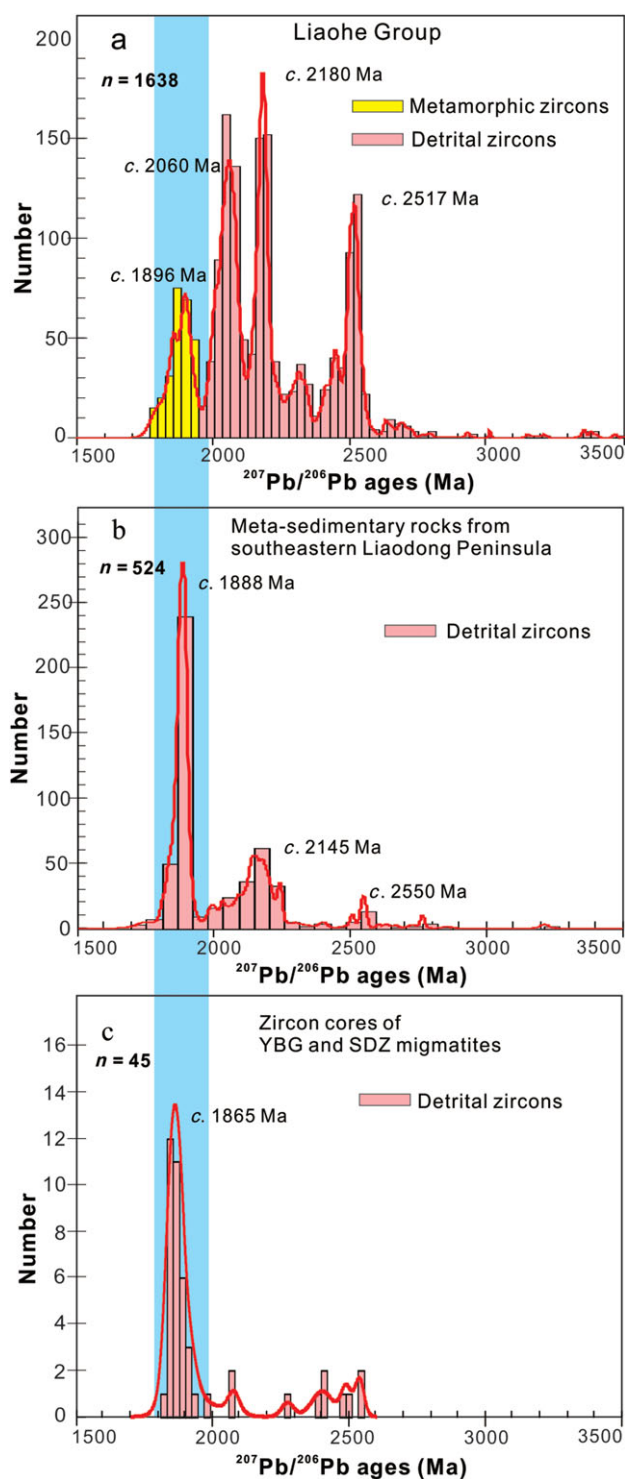


Fig. 12. (Colour online) Summary histogram of the reported zircon ages for (a) the Liaohe Group in the northern and central JLJB, (b) the meta-sedimentary rocks from the southeastern Liaodong Peninsula and (c) YBG and SDZ migmatites. Data from Luo *et al.* (2004, 2008), Meng *et al.* (2013, 2017a, b), Li *et al.* (2015), Liu *et al.* (2018) and Wang *et al.* (2018).

Zhu *et al.* 2011, 2012a, b; Zheng *et al.* 2018). Variable models have been proposed to illustrate the mechanisms, such as delamination of the lower crust (Gao *et al.* 2004, 2008, 2009; Wu *et al.* 2005), underplating of the asthenosphere (Xu, 2001; Zheng *et al.* 2005) and the effects of Pacific Plate subduction (Zheng & Wu, 2009;

Zhu & Zheng, 2009; Zhu *et al.* 2011, 2012a, b; Wu *et al.* 2014; Zheng *et al.* 2018). Regardless of the different models, partial melting in 173–125 Ma in the SE Liaodong Peninsula was intimately related to lithospheric thinning and craton destruction. For the first time, we have reported Mesozoic anatexis in this area. This conclusion is consistent with the coeval magmatism and extensional features (e.g. MCCs, ductile shear zones and fault basins) reported in the SE Liaodong Peninsula (Wu *et al.* 2005; Liu *et al.* 2008, 2011, 2013; Yang & Wu, 2009; Lin *et al.* 2011; Shen *et al.* 2011).

Geochronological studies have documented three major magmatic events in the Liaodong Peninsula during Late Triassic (233–212 Ma), Jurassic (180–156 Ma) and Early Cretaceous (131–117 Ma) time (Wu *et al.* 2005; Yang *et al.* 2007a, b, 2012) (Fig. 14). The two ages of leucosome crystallization reported in the present study (173–161 Ma and 125 Ma) are consistent with the Jurassic–Cretaceous magmatism in the Liaodong Peninsula. Field observations of leucocratic veins and dykes at a high angle to layering are indicative of the migration of anatectic melts. These melts may therefore have contributed to the Jurassic–Cretaceous magmatism, and the relationship between the anatectic melts and the Jurassic–Cretaceous igneous rocks requires further investigation.

Traditionally, anatexis was considered to occur during upper amphibolite- to granulite-facies metamorphism associated with the crustal thickening during orogeny (Brown, 2001; Sawyer, 2001, 2008; Kelsey *et al.* 2008). In the past, Jurassic–Cretaceous amphibolites and granulites have not been reported in the eastern NCC. Migmatites are common within low-angle detachment faults and shear zones related to MCCs in the Liaodong Peninsula. Wang *et al.* (2015) inferred that high local thermal gradients and asymmetric strain localization might have played a key role in the formation of these MCCs. Anatexis at 173–161 Ma and 125 Ma may therefore be related to formation of the MCCs.

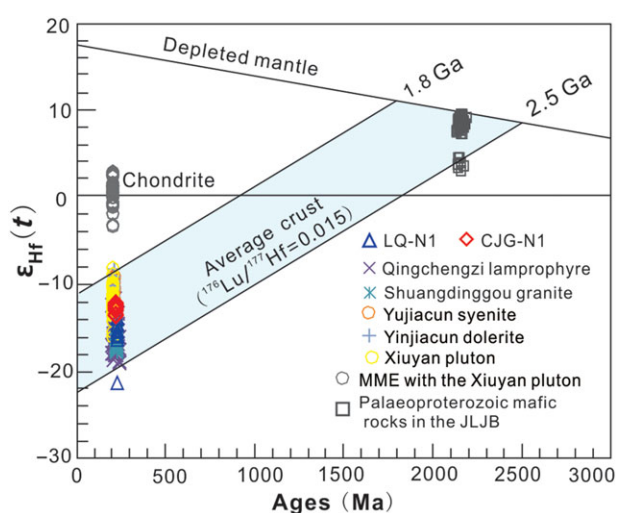
Muscovite and biotite are the most common hydrous reactants that contribute to fluid-absent melting (Weinberg & Hasalová, 2015). Petrological observations indicate that biotite and muscovite experienced breakdown during the partial melting (Figs 3–6). Biotite fluid-absent melting typically occurs at 750–850°C (Patiño Douce & Johnston, 1991; Skjerlie & Johnston, 1993; Weinberg & Hasalová, 2015). However, as mentioned above, it is likely that the migmatites were produced by shallow partial melting of metasedimentary rocks and diorites. Temperatures of 750°C–850°C are higher than those expected in the shallow crust, even in the presence of a thermal anomaly, so other factors must have reduced the reaction temperature.

Previous studies have found that water-rich fluids decrease melting temperatures (Yardley & Barber, 1991; Weinberg & Hasalová, 2015) and increase the rate of melting (Rubie, 1986; Acosta-Vigil *et al.* 2006). Metamorphic reactions commonly preserve metastable assemblages at temperatures of < 500°C, with reaction progress depending on the amount of free fluid available (Wang *et al.* 2015). Anatectic zircons from sample CJG-N1 have high Th/U ratios (0.11–0.76), similar to zircons formed by recrystallization under fluid-rich conditions (Pidgeon, 1992; Rubatto & Hermann, 2003; Dong *et al.* 2017). If anatexis occurred within the shear zones, as discussed above, fluids might infiltrate the rocks to enhance the melting. A water-rich fluid phase may therefore have played a critical role in anatexis at 173–161 Ma and 125 Ma.

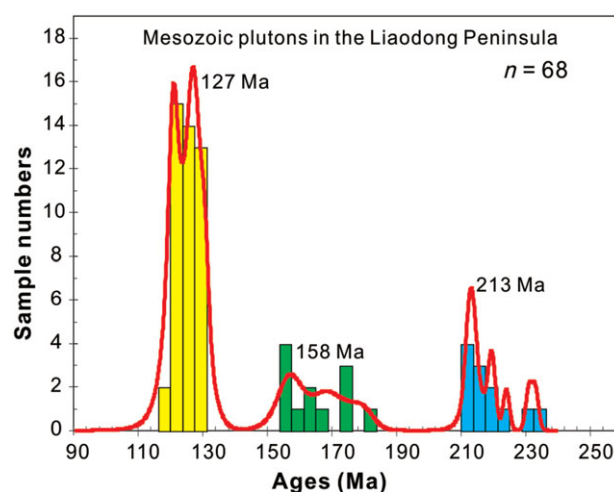
The host rocks of the YBG and SDZ migmatites, which have a greywacke protolith, commonly have peritectic sillimanite, epidote and titanite adjacent to relict biotite, or along the contacts between

Table 2. Summary of geochronological data for the Late Triassic igneous rocks in the Liaodong Peninsula. LA-ICP-MS – laser ablation inductively coupled plasma mass spectrometry; TIMS – thermal ionization mass spectrometry

Sample no.	Sample location	Name of pluton	Rock type	Method	Age (Ma)	Reference
FW01-75	40° 18' 34" N, 123° 12' 42" E	Xiuyan	Monzogranite	TIMS	213 ± 1	Wu <i>et al.</i> (2005)
FW04-324	40° 18' 21" N, 123° 13' 47" E	Xiuyan	Monzogranite	LA-ICP-MS	210 ± 1	Yang <i>et al.</i> (2007b)
FW04-325	40° 18' 21" N, 123° 13' 47" E	Xiuyan	Monzogranite	LA-ICP-MS	211 ± 1	Yang <i>et al.</i> (2007b)
FW04-326	40° 18' 21" N, 123° 13' 47" E	Xiuyan	Diorite	LA-ICP-MS	210 ± 1	Yang <i>et al.</i> (2007b)
FW02-63	40° 18' 49" N, 123° 16' 47" E	Dongjiapuzi	Diorite	LA-ICP-MS	214 ± 2	Yang <i>et al.</i> (2007b)
FW01-92	42° 38' 27" N, 123° 31' 39" E	Shuangyashan	Porphyric granite	TIMS	224 ± 1	Wu <i>et al.</i> (2005)
FW01-94	42° 35' 14" N, 123° 33' 01" E	Laojiandingzi	Diorite	TIMS	220 ± 1	Wu <i>et al.</i> (2005)
013JH011	39° 04' 59" N, 121° 47' 47" E	Daheshangshan	Dolerite	SHRIMP	212 ± 1	Yang <i>et al.</i> (2007a)
03JH021	38° 45' 42" N, 121° 07' 42" E	Yujiacun	Syenite	LA-ICP-MS	221 ± 1	Wu <i>et al.</i> (2005)
03JH025	38° 45' 42" N, 121° 07' 44" E	Yinjiacun	Dolerite	SHRIMP	213 ± 5	Yang <i>et al.</i> (2007a)
FW01-424	40° 57' 40" N, 124° 16' 08" E	Saima	Nepheline syenite	TIMS	233 ± 1	Wu <i>et al.</i> (2005)
FW04-332	40° 54' 39" N, 124° 32' 56" E	Bolinchuan	Nepheline syenite	LA-ICP-MS	231 ± 1	Wu <i>et al.</i> (2005)
QCZ-12	Qingchengzi	Qingchengzi	Lamprophyre	LA-ICP-MS	217 ± 4	Duan <i>et al.</i> (2014)
QCZ-13	Qingchengzi	Qingchengzi	Lamprophyre	LA-ICP-MS	224 ± 4	Duan <i>et al.</i> (2014)
QCZ-15	Qingchengzi	Qingchengzi	Lamprophyre	LA-ICP-MS	210 ± 3	Duan <i>et al.</i> (2014)
QCZ-16	Qingchengzi	Qingchengzi	Lamprophyre	LA-ICP-MS	218 ± 3	Duan <i>et al.</i> (2014)
QCZ-18	Qingchengzi	Qingchengzi	Lamprophyre	LA-ICP-MS	227 ± 5	Duan <i>et al.</i> (2014)
QCZ3-1	Qingchengzi	Shuangdinggou	Monzogranite	LA-ICP-MS	224 ± 1	Duan <i>et al.</i> (2014)
DHKZR1	40° 32' 55" N, 123° 34' 16" E	Daheikeng	Diorite	LA-ICP-MS	220 ± 1	Wang <i>et al.</i> (2019)
HGLZR1	40° 39' 48" N, 123° 34' 01" E	Houbiangou	Monzogranite	LA-ICP-MS	221 ± 1	Wang <i>et al.</i> (2019)
CJG-N1	40° 08' 00" N, 123° 45' 31" E	Congjiagou	Diorite	LA-ICP-MS	221 ± 2	This study
LQ-N1	40° 07' 00" N, 123° 46' 53" E	Lanqi	Diorite	LA-ICP-MS	224 ± 2	This study

**Fig. 13.** (Colour online) $\epsilon_{\text{Hf}}(t)$ v. age diagram for the sample CJG-N1 and LQ-N1 and analysed Triassic igneous rocks from the Liaodong Peninsula. Published data from Yang *et al.* (2007a, b) and Duan *et al.* (2014).

quartz and plagioclase (Figs 3, 5). This relationship suggests that the melting reaction was (biotite or muscovite) + quartz + plagioclase + H_2O -rich fluid = sillimanite + epidote + melt \pm titanite \pm ilmenite. Brown (1979) and Milord *et al.* (2001) describe

**Fig. 14.** (Colour online) Age histogram of the published Mesozoic plutons in the Liaodong Peninsula.

similar relationships in rocks from St Malo, France, where a greywacke protolith underwent fluid-present local anatexis under upper amphibolite-facies conditions without formation of peritectic cordierite or garnet. The host rocks of the LQ and CJG migmatites commonly have peritectic hornblende, titanite, orthopyroxene and K-feldspar on the reactant grain boundaries

(Figs 4, 6), which are aligned parallel to the foliation. The peritectic hornblende contains biotite, plagioclase and quartz inclusions, consistent with water-fluxed melting (Weinberg & Hasalová, 2015). Brown (2013) inferred that mica- and hornblende-bearing leucosomes in host rocks that lack anhydrous minerals are likely to have formed by fluid-present melting. Gardien *et al.* (2000) suggested that hornblende forms only during melt production in the presence of external water. The following melting reactions are proposed for the LQ and CJG migmatites, based on the above observations, experimental results and thermodynamic modelling of diorites and granodiorites (e.g. Escuder-Viruete, 1999; Slagstad *et al.* 2005; Cherneva & Georgieva, 2007; Reichardt & Weinberg, 2012): (1) biotite + quartz + plagioclase + H₂O-rich fluid = orthopyroxene + K-feldspar + melt; and (2) biotite + quartz + plagioclase + H₂O-rich fluid = hornblende + K-feldspar + titanite + melt ± orthopyroxene ± rutile.

In summary, anatexis at 173–161 Ma and 125 Ma is inferred to have been associated with the breakdown of muscovite and biotite in the presence of a water-rich fluid. Locally, a thermal anomaly and strain softening facilitated partial melting. Lithospheric thinning of the NCC provides a broader geodynamic setting for this anatexis event.

7. Conclusions

- (1) Geochronological and geochemical evidence indicates that the protoliths of the SDZ and YBG migmatites were metagreywackes that were deposited sometime after *c.* 1857 Ma. The protoliths of the CJG and LQ migmatites were the Upper Triassic (*c.* 224–221 Ma) diorites formed by partial melting of recycled ancient crust.
- (2) Anatexis occurred at 173–161 Ma and 125 Ma as a consequence of the breakdown of muscovite and biotite in the presence of water-rich fluid under an anomalous thermal regime.
- (3) The 173–161 Ma and 125 Ma anatectic events most likely resulted from the Mesozoic lithospheric thinning of the NCC. Newly generated melts further weakened the crust and enhanced the regional extension.

Acknowledgements. We are grateful to editor Dr Kathryn Goodenough and two anonymous reviewers for their thorough and insightful reviews and valuable suggestions to improve the quality of our manuscript. This study was jointly funded by the Fundamental Research Funds for the Central Universities (grant nos 32110-31650011 and 32110-31610343), the China Postdoctoral Science Foundation (grant no. 2018M633210) and the 12th Chinese 1000 Young Talents Program (2016-67, grant no. 32020002).

Declaration of Interest. None.

Supplementary material. To view supplementary material for this article, please visit <https://doi.org/10.1017/S0016756820000552>

References

- Acosta-Vigil A, London D and Morgan GB (2006) Experiments on the kinetics of partial melting of a leucogranite at 200 MPa H₂O and 690–800°C: compositional variability of melts during the onset of H₂O-saturated crustal anatexis. *Contributions to Mineralogy and Petrology* **151**, 539–57.
- Brown M (1979) The petrogenesis of the St. Malo migmatite belt, Armorican Massif, France, with particular reference to the diatexites. *Neues Jahrbuch für Mineralogie-Abhandlungen* **135**, 48–74.
- Brown M (1994) The generation, segregation, ascent and emplacement of granite magma: the migmatite-to-crustally-derived granite connection in thickened orogens. *Earth-Science Reviews* **36**, 83–130.
- Brown M (2001) Orogeny, migmatites and leucogranites: a review. *Journal of Earth System Science* **110**, 313–36.
- Brown M (2013) Granite: from genesis to emplacement. *Bulletin of the Geological Society of America* **125**, 1079–113.
- Cai JH, Yan GH, Mu BL, Xu BL, Shao HX and Xu RH (2002) U-Pb and Sm-Nd isotopic ages of an alkaline syenite complex body in Liangtun-Kuangdongguo, Gai County of Liaoning Province and their geological significance. *Acta Petrologica Sinica* **18**, 349–354 (in Chinese with English abstract).
- Cavalcante GCG, Viegas G, Archanjo CJ and Da Silva ME (2016) The influence of partial melting and melt migration on the rheology of the continental crust. *Journal of Geodynamics* **101**, 186–99.
- Cherneva Z and Georgieva M (2007) Amphibole-bearing leucosome from the Chepelare area, Central Rhodopes: P-T conditions of melting and crystallization. *Geochemistry, Petrology and Mineralogy* **45**, 79–95.
- Dong CY, Xie HQ, Kröner A, Wang SJ, Liu SJ, Xie SW, Song ZY, Ma MZ, Liu DY and Wan YS (2017) The complexities of zircon crystallization and overprinting during metamorphism and anatexis: an example from the late Archean TTG terrane of western Shandong Province, China. *Precambrian Research* **300**, 181–200.
- Duan XX, Zeng QD, Yang JH, Liu JM, Wang YB and Zhou LL (2014) Geochronology, geochemistry and Hf isotope of Late Triassic magmatic rocks of Qingchengzi district in Liaodong peninsula, Northeast China. *Journal of Asian Earth Sciences* **91**, 107–24.
- Escuder-Viruete J (1999) Hornblende-bearing leucosome development during synorogenic crustal extension in the Tormes Gneiss Dome, NW Iberian Massif, Spain. *Lithos* **46**, 751–72.
- Gao S, Rudnick RL, Xu WL, Yuan HL, Liu YS, Walker RJ, Puchtel IS, Liu X, Huang H, Wang XR and Yang J (2008) Recycling deep cratonic lithosphere and generation of intraplate magmatism in the North China Craton. *Earth Planetary Science Letters* **270**, 41–53.
- Gao S, Rudnick RL, Yuan HL, Liu XM, Liu YS, Xu WL, Ling WL, Ayers J, Wang XC and Wang QH (2004) Recycling lower continental crust in the North China craton. *Nature* **432**, 892–97.
- Gao S, Zhang JF, Xu WL and Liu YS (2009) Delamination and destruction of the North China Craton. *Chinese Science Bulletin* **54**, 3367.
- Gardien V, Thompson AB and Ulmer P (2000) Melting of biotite + plagioclase + quartz gneisses; the role of H₂O in the stability of amphibole. *Journal of Petrology* **41**, 651–66.
- Kelsey DE, Clark C and Hand M (2008) Thermobarometric modelling of zircon and monazite growth in melt-bearing systems: examples using model metapelitic and metapsammitic granulites. *Journal of Metamorphic Geology* **26**, 199–212.
- Li SZ, Zhao GC, Santosh M, Liu X, Dai L, Suo YH, Tam PK, Song M and Wang PC (2012) Paleoproterozoic structural evolution of the southern segment of the Jiao-Liao-Ji belt, North China Craton. *Precambrian Research* **200–203**, 59–73.
- Li SZ, Zhao GC, Sun M, Han ZZ, Hao DF, Luo Y and Xia XP (2005) Deformation history of the Paleoproterozoic Liaohe Group in the Eastern Block of the North China Craton. *Journal of Asian Earth Sciences* **24**, 659–74.
- Li Z, Chen B, Wei CJ, Wang CX and Han W (2015) Provenance and tectonic setting of the Paleoproterozoic metasedimentary rocks from the Liaohe Group, Jiao-Liao-Ji Belt, North China Craton: insights from detrital zircon U-Pb geochronology, whole-rock Sm-Nd isotopes, and geochemistry. *Journal of Asian Earth Sciences* **111**, 711–32.
- Lin W, Monié P, Faure M, Schärer U, Shi YH and Breton NL (2011) Cooling paths of the NE China crust during the Mesozoic extensional tectonics: example from the south-Liaodong peninsula metamorphic core complex. *Journal of Asian Earth Sciences* **42**, 1048–65.
- Liu DY, Nutman AP, Compston W, Wu JS and Shen QH (1992) Remnants of ≥3800Ma crust in the Chinese part of the Sino-Korean Craton. *Geology* **20**, 339–42.
- Liu FL, Liu CH, Itano K, Iizuka T, Cai J and Wang F (2017a) Geochemistry, U-Pb dating, and Lu-Hf isotopes of zircon and monazite of porphyritic granites within the Jiao-Liao-Ji orogenic belt: implications for petrogenesis and tectonic setting. *Precambrian Research* **300**, 78–106.

- Liu FL, Liu PH, Wang F, Liu CH and Cai J (2015) Progresses and overviews of voluminous meta-sedimentary series within the Paleoproterozoic Jiao-Liao-Ji orogenic/mobile belt, North China Craton. *Acta Petrologica Sinica* **31**, 2816–46 (in Chinese with English abstract).
- Liu J, Liu ZH, Zhao C, Wang CJ and Peng YB (2017b) Petrogenesis and zircon U–Pb LA–ICP–MS dating of newly discovered Mesoproterozoic tonalitic gneiss in the Luanjiajie area of northern Liaoning Province, China. *International Geology Review* **59**, 1575–89.
- Liu J, Zhang J, Liu ZH, Yin CQ, Zhao C, Li Z, Yang ZJ and Dou SY (2018) Geochemical and geochronological study on the Paleoproterozoic rock assemblage of the Xiuyan region: new constraints on an integrated rift-and-collision tectonic process involving the evolution of the Jiao-Liao-Ji Belt, North China Craton. *Precambrian Research* **310**, 179–97.
- Liu JL, Davis GA, Ji M, Guan H and Bai X (2008) Crustal detachment and destruction of the keel of North China Craton: constraints from Late Mesozoic Extensional Structures. *Earth Science Frontiers* **15**, 72–81.
- Liu JL, Ji M, Shen L, Guan HM and Davis GA (2011) Early Cretaceous extensional structures in the Liaodong Peninsula: structural associations, geochronological constraints and regional tectonic implications. *Science China Earth Sciences* **54**, 823–42.
- Liu JL, Shen L, Ji M, Guan HM, Zhang ZC and Zhao ZD (2013) The Liaonan/Wanfu metamorphic core complexes in the Liaodong Peninsula: two stages of exhumation and constraints on the destruction of the North China Craton. *Tectonics* **32**, 1121–41.
- Liu YS, Gao S, Hu ZC, Gao CG, Zong KQ and Wang DB (2010) Continental and oceanic crust recycling-induced melt-peridotite interactions in the Trans-North China Orogen. U–Pb dating, Hf isotopes and trace elements in zircons from mantle xenoliths. *Journal of Petrology* **51**, 537–71.
- Lu XP, Wu FY, Guo JH, Wilde SA, Yang JH, Liu XM and Zhang XO (2006) Zircon U–Pb geochronological constraints on the Paleoproterozoic crustal evolution of the Eastern Block in the North China Craton. *Precambrian Research* **146**, 138–64.
- Lu XP, Wu FY, Lin JQ, Sun DY, Zhang YB and Guo CL (2004) Geochronological successions of the Early Precambrian granitic magmatism in southern Liaoning Peninsula and its constraints on tectonic evolution of the North China Craton. *Chinese Journal of Geology* **39**, 123–39 (in Chinese with English abstract).
- Luo Y, Sun M, Zhao GC, Li SZ, Ayers JC, Xia XP and Zhang JH (2008) A comparison of U–Pb and Hf isotopic compositions of detrital zircons from the North and South Liaohe Groups: constraints on the evolution of the Jiao–Liao–Ji Belt, North China Craton. *Precambrian Research* **163**, 279–306.
- Luo Y, Sun M, Zhao GC, Li SZ, Xu P, Ye K and Xia XP (2004) LA–ICP–MS U–Pb zircon ages of the Liaohe Group in the Eastern Block of the North China Craton: constraints on the evolution of the Jiao–Liao–Ji Belt. *Precambrian Research* **134**, 349–71.
- McLennan SM, Taylor SR and McCulloch MT (1990) Geochemical and Nd–Sr isotopic composition of deep-sea turbidites: crystal evolution and plate tectonic associations. *Geochimica et Cosmochimica Acta* **54**, 2015–50.
- Meng E, Liu FL, Cui Y and Cai J (2013) Zircon U–Pb and Lu–Hf isotopic and whole-rock geochemical constraints on the protolith and tectonic history of the Changhai metamorphic supracrustal sequence in the Jiao-Liao-Ji Belt, southeast Liaoning Province, northeast China. *Precambrian Research* **233**, 297–315.
- Meng E, Liu FL, Liu PH, Liu CH, Yang H, Wang F, Shi JR and Cai J (2014) Petrogenesis and tectonic significance of Paleoproterozoic meta-mafic rocks from central Liaodong Peninsula, northeast China: evidence from zircon U–Pb dating and in situ Lu–Hf isotopes, and whole-rock geochemistry. *Precambrian Research* **247**, 92–109.
- Meng E, Wang CY, Li YG, Li Z, Yang H, Cai J, Ji L and Ji MQ (2017a) Zircon U–Pb–Hf isotopic and whole-rock geochemical studies of Paleoproterozoic metasedimentary rocks in the northern segment of the Jiao-Liao-Ji Belt, China: implications for provenance and regional tectonic evolution. *Precambrian Research* **298**, 472–89.
- Meng E, Wang CY, Yang H, Cai J, Ji L and Li YG (2017b) Paleoproterozoic metavolcanic rocks in the Ji'an Group and constraints on the formation and evolution of the northern segment of the Jiao-Liao-Ji Belt, China. *Precambrian Research* **294**, 133–50.
- Milord I, Sawyer EW and Brown M (2001) Formation of diatexite migmatite and granite magma during anatexis of semi-pelitic metasedimentary rocks: an example from St. Malo, France. *Journal of Petrology* **42**, 487–505.
- Patiño Douce AE and Johnston AD (1991) Phase equilibria and melt productivity in the pelitic system: implications for the origin of peraluminous granulites and aluminous granulites. *Contributions to Mineralogy and Petrology* **107**, 202–18.
- Pidgeon RT (1992) Recrystallisation of oscillatory zoned zircon: some geochronological and petrological implications. *Contributions to Mineralogy and Petrology* **110**, 463–72.
- Qi L, Hu J and Gregoire DC (2000) Determination of trace elements in granites by inductively coupled plasma-mass spectrometry. *Talanta* **51**, 507–13.
- Reichardt H and Weinberg RF (2012) Hornblende chemistry in meta- and diatexites and its retention in the source of leucogranites: an example from the Karakoram shear Zone, NW India. *Journal of Petrology* **53**, 1287–318.
- Rickwood PC (1989) Boundary lines within petrologic diagrams which use oxides of major and minor elements. *Lithos* **22**, 247–63.
- Rubatto D and Hermann J (2003) Zircon formation during fluid circulation in eclogites (Monviso, Western Alps): implications for Zr and Hf budget in subduction zones. *Geochimica et Cosmochimica Acta* **67**, 2173–218.
- Rubie DC (1986) The catalysis of mineral reactions by water and restrictions on the presence of aqueous fluid during metamorphism. *Mineralogical Magazine* **50**, 399–415.
- Rudnick RL and Gao S (2003) Composition of the continental crust. In *The Crust* (ed. RL Rudnick), pp. 1–64. Amsterdam: Elsevier, Treatise in Geochemistry no. 3.
- Sawyer EW (2001) Melt segregation in the continental crust: distribution and movement of melt in anatectic rocks. *Journal of Metamorphic Geology* **19**, 291–309.
- Sawyer EW (2008) *Atlas of Migmatites*. Ottawa, Ontario: NRC Research Press, The Canadian Mineralogist, Special Publication no. 9.
- Simonen A (1953) Stratigraphy and sedimentation of the Svecofennide, early Archean supracrustal rocks in southwestern Finland. *Bulletin of the Geological Society of Finland* **160**, 1–64.
- Shen L, Liu JL, Hu L, Ji M, Guan HM and Davis GA (2011) The Dayingzi detachment fault system in Liaodong Peninsula and its regional tectonic significance. *Science China Earth Sciences* **54**, 1469–83.
- Skjerlie KP and Johnston AD (1993) Fluid-absent melting behavior of an F-rich tonalitic gneiss at mid-crustal pressures: implications for the generation of anorogenic granites. *Journal of Petrology* **34**, 785–815.
- Slagstad T, Jamieson RA and Culshaw NG (2005) Formation, crystallization, and migration of melt in the mid-orogenic crust. Muskoka Domain migmatites, Grenville Province, Ontario. *Journal of Petrology* **46**, 893–919.
- Solari LA, Gómez-Tuena A, Bernal JP, Pérez-Arvizu O and Tanner M (2010) U–Pb zircon geochronology with an integrated LA–ICP–MS microanalytical workstation: achievements in precision and accuracy. *Geostandards and Geoanalytical Research* **34**, 5–18.
- Sun SS and McDonough WF (1989) Chemical and isotopic systematics of oceanic basalts: implications for mantle composition and processes. In *Magmatism in the Ocean Basins* (eds AD Saunders and MJ Norry), pp. 313–45. Geological Society of London, Special Publication no. 42.
- Wan YS, Liu DY, Nutman AP, Zhou HY, Dong CY, Yin XY and Ma MZ (2012) Multiple 3.8–3.1 Ga tectono-magmatic events in a newly discovered area. *Journal of Asian Earth Sciences* **54–55**, 18–30.
- Wan YS, Liu DY, Yin XY, Wilde SA, Xie LW, Yang YH, Zhou HY and Wu JS (2007) SHRIMP geochronology and Hf isotope composition of zircons from the Tiejiaoshan granite and supracrustal rocks in the Anshan area, Liaoning Province. *Acta Petrologica Sinica* **23**, 241–52 (in Chinese with English abstract).
- Wan YS, Ma MZ, Dong CY and Liu DY (2015) Widespread late Neoproterozoic reworking of Meso- to Paleoproterozoic continental crust in the Anshan-Benxi area, North China Craton, as documented by U–Pb–Nd–Hf–O isotopes. *American Journal of Science* **315**, 620–70.
- Wang F, Liu FL, Liu PH, Cai J, Ji L, Liu LS and Tian ZH (2018) Redefinition of the Gaixian Formation of the South Liaohe Group: evidence from the detrital zircon U–Pb geochronology of metamorphosed sandstone in Huanghuadian–Suzigou area, the southern Liaoning Province. *Acta Petrologica Sinica* **34**, 1219–28 (in Chinese with English abstract).

- Wang K, Burov E, Gumiaux C, Chen Y, Lu G, Mezri L and Zhao L (2015) Formation of metamorphic core complexes in non-over-thickened continental crust: a case study of Liaodong Peninsula (East Asia). *Lithos* **238**, 86–100.
- Wang RM, He GP, Chen ZZ, Zheng SY and Geng YS (1987) *Graphical Method for Protolith Reconstruction of Metamorphic Rocks*. Beijing: Geological Publishing House, 51 p.
- Wang W, Liu SW, Cawood PA, Bai X, Guo RR, Guo B and Wang K (2016) Late Neoproterozoic subduction-related crustal growth in the Northern Liaoning region of the North China Craton: evidence from ~2.55 to 2.50 Ga granitoid gneisses. *Precambrian Research* **281**, 200–23.
- Wang XL, Lv X, Liu YJ, Zhao YY, Li C, Wu WB, Wang YP and Li HY (2019) LA-ICP-MS zircon U-Pb ages, geochemical characteristics of Late Triassic intrusives in Xiuyan area, eastern Liaoning and their geological significances. *Geological Review* **65**, 401–16 (in Chinese with English abstract).
- Wang XP, Peng P, Wang C and Yang SY (2017) Nature of three episodes of Paleoproterozoic magmatism (2180 Ma, 2115 Ma and 1890 Ma) in the Liaoji belt, North China with implications for tectonic evolution. *Precambrian Research* **298**, 252–67.
- Weinberg RF and Hasalová P (2015) Water-fluxed melting of the continental crust: a review. *Lithos* **212–215**, 158–88.
- Winchester JA and Floyd PA (1977) Geochemical discrimination of different magma series and their differentiation products using immobile elements. *Chemical Geology* **20**, 325–43.
- Wu FY, Lin JQ, Wilde S, Zhang XO and Yang JH (2005) Nature and significance of the Early Cretaceous giant igneous event in eastern China. *Earth and Planetary Science Letters* **233**, 103–19.
- Wu FY, Xu YG, Zhu RX and Zhang GW (2014) Thinning and destruction of the cratonic lithosphere: a global perspective. *Science China Earth Sciences* **57**, 2878–90.
- Wu FY, Yang YH, Xie LW, Yang JH and Xu P (2006) Hf isotopic compositions of the standard zircons and baddeleyites used in U-Pb geochronology. *Chemical Geology* **234**, 105–26.
- Xu W and Liu FL (2019) Geochronological and geochemical insights into the tectonic evolution of the Paleoproterozoic Jiao-Liao-Ji belt, Sino-Korean Craton. *Earth-Science Reviews* **193**, 162–98.
- Xu YG (2001) Thermo-tectonic destruction of the Archean lithospheric keel beneath the Sino-Korean Craton in China: evidence, timing and mechanism. *Physics and Chemistry of the Earth, Part A: Solid Earth and Geodesy* **26**, 747–57.
- Yakymchuk C and Brown M (2014) Behaviour of zircon and monazite during crustal melting. *Journal of the Geological Society of London* **171**, 465–79.
- Yang JH, Sun JF, Chen FK, Wilde SA and Wu FY (2007a) Sources and petrogenesis of Late Triassic dolerite dikes in the Liaodong Peninsula: implications for post-collisional lithosphere thinning of Eastern North China Craton. *Journal of Petrology* **48**, 1973–97.
- Yang JH, Sun JF, Zhang JH and Wilde SA (2012) Petrogenesis of Late Triassic intrusive rocks in the northern Liaodong Peninsula related to decratonization of the North China Craton: zircon U-Pb age and Hf-O isotope evidence. *Lithos* **153**, 108–28.
- Yang JH and Wu FY (2009) Triassic magmatism and its relation to decratonization in the eastern North China Craton. *Science in China Series D: Earth Sciences* **52**, 1319–30.
- Yang JH, Wu FY, Wilde SA and Liu XM (2007b) Petrogenesis of Late Triassic granitoids and their enclaves with implications for post-collisional lithospheric thinning of the Liaodong Peninsula, North China Craton. *Chemical Geology* **242**, 155–75.
- Yang JH, Wu FY, Xie LW and Liu XM (2007c) Petrogenesis and tectonic implications of Kuangdonggou syenites in the Liaodong peninsula, east North China Craton; constraints from in-situ zircon U-Pb ages and Hf isotopes. *Acta Petrologica Sinica* **23**, 263–76 (in Chinese with English abstract).
- Yardley BWD and Barber JP (1991) Melting reactions in the Connemara Schists: the role of water infiltration in the formation of amphibolite facies migmatites. *American Mineralogist* **76**, 848–56.
- Yin A and Nie S (1996) Phanerozoic palinspastic reconstruction of China and its neighboring regions. In *The Tectonic Evolution of Asia* (eds A Yin and TM Harrison), pp. 285–442. Cambridge: Cambridge University Press.
- Zhai MG (2016) Comparative study of geology in North China and Korean Peninsula: research advances and key issues. *Acta Petrologica Sinica* **32**, 2915–32 (in Chinese with English abstract).
- Zhai MG, Zhang XH, Zhang YB, Wu FY, Peng P, Li QL, Li Z, Guo JH, Li TS, Zhao L, Zhou LG and Zhu XY (2019) The geology of North Korea: an overview. *Earth-Science Reviews* **194**, 57–96.
- Zhang HF (2009) Peridotite-melt interaction: a key point for the destruction of cratonic lithospheric mantle. *Chinese Science Bulletin* **54**, 3417.
- Zhang HF, Sun M, Zhou XH, Fan WM, Zhai MG and Yin JF (2002) Mesozoic lithosphere destruction beneath the North China Craton: evidence from major-, trace-element and Sr-Nd-Pb isotope studies of Fangcheng basalts. *Contributions to Mineralogy and Petrology* **144**, 241–53.
- Zhang J, Zhao GC, Li SZ, Sun M, Chan LS and Shen WL (2012) Structural pattern of the Wutai complex and its constraints on the tectonic framework of the Trans-North China Orogen. *Precambrian Research* **222–223**, 212–29.
- Zhang J, Zhao GC, Li SZ, Sun M, Liu SW, Wilde SA, Kröner A and Yin CQ (2007) Deformation history of the Hengshan complex: implications for the tectonic evolution of the Trans-North China Orogen. *Journal of Structural Geology* **29**, 933–49.
- Zhang J, Zhao GC, Li SZ, Sun M, Wilde SA, Liu SW and Yin CQ (2009) Polyphase deformation of the Fuping complex, Trans-North China Orogen: structures, SHRIMP U-Pb zircon ages and tectonic implications. *Journal of Structural Geology* **31**, 177–93.
- Zhang QS and Yang ZS (1988) *Early Crust and Mineral Deposits of Liaodong Peninsula*. Beijing: Geological Publishing House, pp. 218–450 (in Chinese with English abstract).
- Zhang SH, Zhao Y, Davis GA, Ye H and Wu F (2014) Temporal and spatial variations of Mesozoic magmatism and deformation in the North China Craton: implications for lithospheric thinning and decratonization. *Earth-Science Reviews* **131**, 49–87.
- Zhao GC, Peter AC, Li SZ, Wilde SA, Sun M, Zhang J, He YJ and Yin CQ (2012) Amalgamation of the North China Craton: key issues and discussion. *Precambrian Research* **222–223**, 55–76.
- Zhao GC, Sun M, Wilde SA and Li SZ (2005) Late Archean to Paleoproterozoic evolution of the North China Craton: key issues revisited. *Precambrian Research* **136**, 177–202.
- Zhao R, Wang QF, Deng J, Santosh M, Liu XF and Cheng HY (2018) Late Mesozoic magmatism and sedimentation in the Liaodong Peninsula: new constraints on lithospheric thinning of the North China Craton. *Lithos* **322**, 312–24.
- Zheng JP, Sun M, Zhou MF and Robinson P (2005) Trace elemental and PGE geochemical constraints of Mesozoic and Cenozoic peridotitic xenoliths on lithospheric evolution of the North China Craton. *Geochimica et Cosmochimica Acta* **69**, 3401–18.
- Zheng YF and Wu FY (2009) Growth and reworking of cratonic lithosphere. *Chinese Science Bulletin* **54**, 3347–53.
- Zheng YF, Xu Z, Zhao ZF and Dai LQ (2018) Mesozoic mafic magmatism in North China: implications for thinning and destruction of cratonic lithosphere. *Science China Earth Sciences* **61**, 353–85.
- Zhong MS, Wu ZJ, Liu J, Zhang GR, Wang Q, Gao FL, Pan YQ and Gao YZ (2019) Comprehensive study of metamorphic core complex in southern Liaodong Peninsula, NE China. *E2S Web of Conferences* **131**, 01032.
- Zhu G, Jian DZ, Zhang BL and Chen Y (2012a) Destruction of the eastern North China Craton in a backarc setting: evidence from crustal deformation kinematics. *Gondwana Research* **22**, 86–103.
- Zhu RX, Chen L, Wu FY and Liu JL (2011) Timing, scale and mechanism of the destruction of the North China Craton. *Science China Earth Sciences* **54**, 789–97.
- Zhu RX, Xu YG, Zhu G, Zhang HF, Xia QK and Zheng TY (2012b) Destruction of the North China Craton. *Science China Earth Science* **55**, 1565–87.
- Zhu RX and Zheng TY (2009) Destruction geodynamics of the North China craton and its Paleoproterozoic plate tectonics. *Chinese Science Bulletin* **54**, 3354–66.